DYNAMIC MODELING AND CASCADED CONTROL FOR A MULTI-EVAPORATOR SUPERMARKET REFRIGERATION SYSTEM

A Thesis

by

ANKUSH GUPTA

Submitted to the Office of Graduate Studies of
Texas A&M University
in partial fulfillment of the requirements for the degree of

MASTER OF SCIENCE

Approved by:

Chair of Committee,	Bryan Rasmussen
Committee Members,	Michael Pate
	Jeff Haberl
Head of Department,	Jerald Caton

December 2012

Major Subject: Mechanical Engineering

ABSTRACT

The survey from US Department of Energy showed that about one-third of energy consumption in US is due to air conditioning and refrigeration systems. This significant usage of electricity in the HVAC industry has prompted researchers to develop dynamic models for the HVAC components, which leads to implementation of better control and optimization techniques. In this research, efforts are made to model a multi-evaporator system. A novel dynamic modeling technique is proposed based on moving boundary method, which can be generalized for any number of evaporators in a vapor compression cycle. The models were validated experimentally on a commercial supermarket refrigeration unit. Simulation results showed that the models capture the major dynamics of the system in both the steady state and transient external disturbances. Furthermore the use of MEMS (microelectromechanical) based Silicon Expansion Valves (SEVs) have reportedly shown power savings as compared to the Thermal Expansion Valves (TEVs). Experimental tests were conducted on a supermarket refrigeration unit fitted with the MEMS valves to explain the cause of these potential energy savings. In this study an advanced cascaded control algorithm was also designed to control the MEMS valves. The performance of the cascaded control architecture was compared with the standard Thermal Expansion Valves (TEVs) and a commercially available Microstaq (MS) Superheat Controller (SHC). The results reveal that the significant efficiency gains derived on the SEVs are due to better superheat regulation, tighter superheat control and superior cooling effects in shorter time period

which reduces the total run-time of the compressor. It was also observed that the duty cycle was least for the cascaded control algorithm. The reduction in duty cycle indicates early shut-off for the compressor resulting in maximum power savings for the cascaded control, followed by the Microstaq controller and then the Thermal Expansion Valves.

DEDICATION

This thesis is dedicated to my parents and friends.

ACKNOWLEDGEMENTS

I would like to acknowledge Department of Energy (DOE) and Microstaq for providing financial support to this research work. I would like to thank my thesis advisor Dr. Bryan Rasmussen for his continuous assistance and guidance throughout my research and development of this thesis. I am also grateful to Dr. Michael Pate and Dr. Jeff Haberl for serving on my advisory committee.

I acknowledge the support of all my colleagues at the Thermo-Fluids Control Laboratory who maintained a lively working environment with fun and laughter. I would especially like to thank Matt Elliott for his valuable suggestions and insightful discussions. Finally, thanks to my parents and friends for their consistence motivation and encouragement.

ABBREVIATIONS

$AC\&R$	Air Conditioning and Refrigeration
AEV	Automatic Expansion Valve
DOE	Department of Energy
EEV	Electronic Expansion Valve
FCV	Finite Control Volume
HEV	Hybrid Expansion Valve
$HVAC\&R$	Heating, Venting, Air Conditioning and Refrigeration
MB	Moving Boundary
$MEMS$	Microelectromechanical System
MS	Microstaq
SEV	Silicon Expansion Valve
SHC	Superheat Controller
TEV	Thermal Expansion Valve
VCC	Vapor Compression Cycle

NOMENCLATURE

	Units	Explanation
A_i	$[m^2]$	Internal surface area of heat exchanger
A_o	$[m^2]$	Internal surface area of heat exchanger
A	$[m^2]$	Cross section area through which air enters the evaporator
C_d	$-$	Coefficient of discharge of the expansion valve
Cp	$[kJ/kgK]$	Specific heat of air
$\left(C_p \rho V\right)_w$	$[kJ/K]$	Thermal capacitance of tube wall per unit length
d	$[m]$	Diameter of the tube
Dh	$[m]$	Hydraulic diameter
f, g	$-$	Continuous functions
h	$[kJ/kg]$	Enthalpy of the refrigerant
k_a	$[\frac{kW}{(m.K)}]$	Thermal conductivity of air
L	$[m]$	Length of liquid phase region in the heat exchanger tube
L_{total}	$[m]$	Total length of heat exchanger tubes
$\dot{m}$	$[kg/s]$	Mass flow rate of air
$\dot{m}_{air}$	$[kg/s]$	Mass flow rate of the air over the evaporator
$\dot{m}_{in}$	$[kg/s]$	Mass flow rate of the refrigerant flowing into the evaporator
$\dot{m}_k$	$[kg/s]$	Mass flow rate of the refrigerant flowing through the compressor

$\dot{m}_{out}$	$[kg/s]$	Mass flow rate of the refrigerant flowing out of the evaporator
$\dot{m}_v$	$[kg/s]$	Mass flow rate of the refrigerant flowing through the valve
Nu	–	Nusselt's number
P	–	Pressure
P_c	$[kPa]$	Condenser pressure
P_e	$[kPa]$	Evaporator pressure
P_{in}	$[kPa]$	Pressure at expansion valve inlet
P_{out}	$[kPa]$	Pressure at expansion valve outlet
Pr	–	Prandlt number
Re	–	Reynolds number
T_a	[°C]	Temperature of air
T_r	[°C]	Temperature of the refrigerant
T_{sat}	[°C]	Saturation temperature
T_w	[°C]	Temperature of heat exchanger tube wall
u	–	Inputs
u_v	[%]	Percentage opening of the SEV
V_k	$[m^3]$	Volume of the compressor
v	$[m/s]$	Velocity of air
x	–	Dynamic states
z	–	Spatial dimension
Z	–	Matrix

α_i	$[\mathrm{W/m^2K}]$	Heat transfer coefficient between tube wall and internal fluid
α_o	$[\mathrm{W/m^2K}]$	Heat transfer coefficient between tube wall and external fluid
η_{vol}	$-$	Volumetric efficiency of the compressor
η_k	$-$	Adiabatic efficiency of the compressor
ρ	$[kg/m^3]$	Density of refrigerant
ρ_l	$[kg/m^3]$	Liquid phase refrigerant density
ρ_g	$[kg/m^3]$	Vapor phase refrigerant energy
$\bar{\gamma}$	$-$	Mean void fraction
μ	$-$	Weight factor for external air temperature

TABLE OF CONTENTS

Page

LIST OF FIGURES

Page

LIST OF TABLES

Page

1. INTRODUCTION

Air conditioning and refrigeration systems accounted for about 20% of the USA's commercial power consumption in 2008 [1]. Food sales and food services are use the maximum amount of energy amongst all commercial buildings. According to the Energy Star building survey, supermarkets use an average of 50 kWh of electricity per square foot per year [2]. With typical supermarkets having a sales area of 3700 - 5600 m^2 [3] the amount of energy consumed by these buildings becomes enormous. Figure 1-1 below shows that supermarkets belong to highly intensive energy sectors.

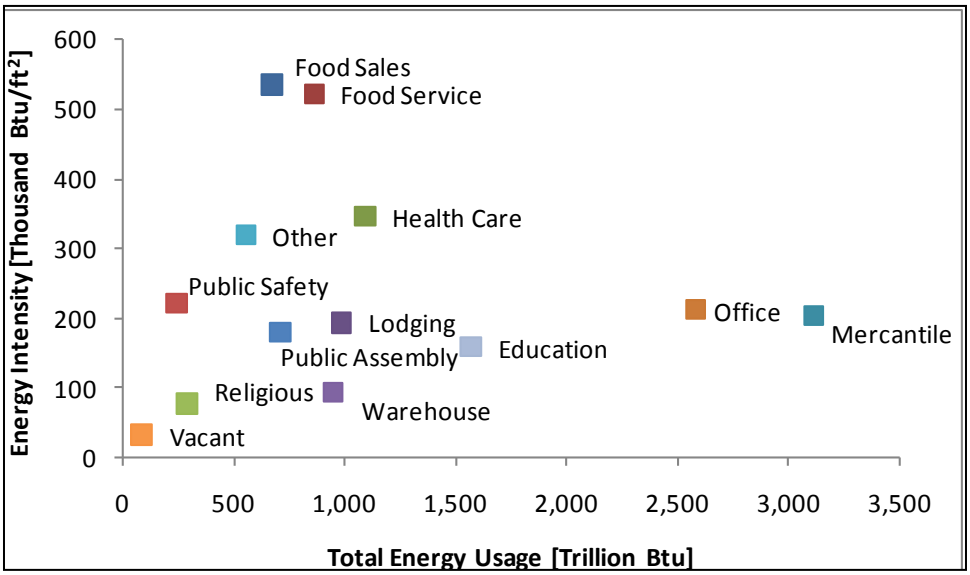

Figure 1-1 Commercial Building Energy Use [4]

Refrigeration is the largest component of supermarket energy consumption. The estimated consumption of energy by refrigeration alone is 60-70% of the total store

energy use [3]. Significant amount of energy is used to maintain the temperature of the fresh food kept in open display cases, glass door display cases, walk-in-coolers and the storage refrigerators. These systems have traditionally been controlled and operated using simple mechanisms and strategies. Recent research has demonstrated that significant efficiency improvements are possible through more sophisticated control and optimization techniques, enabled by electronically controlled components. A microelectromechanical system (MEMS) is the technology of very small devices that is particularly used in the electronic hardware and semi-conductor industry. The use of MEMS valves for fluid control applications has been so far limited to low fluid pressures [5]. However, recent research and development has led to the use of MEMS valves, from low to mid-range fluid pressure applications. Also, the small size and weight of these valves make it more suitable for today's fluid circuitry.

Microstaq, an Austin based manufacturing firm, is the developer of a Silicon Expansion Valve (SEV) and Superheat Controller (SHC) that can be used in air-conditioning and refrigeration systems. Microstaq uses MEMS technology to fabricate these valves. Figure 1-2 gives the prototype of a Silicon Expansion Valve.

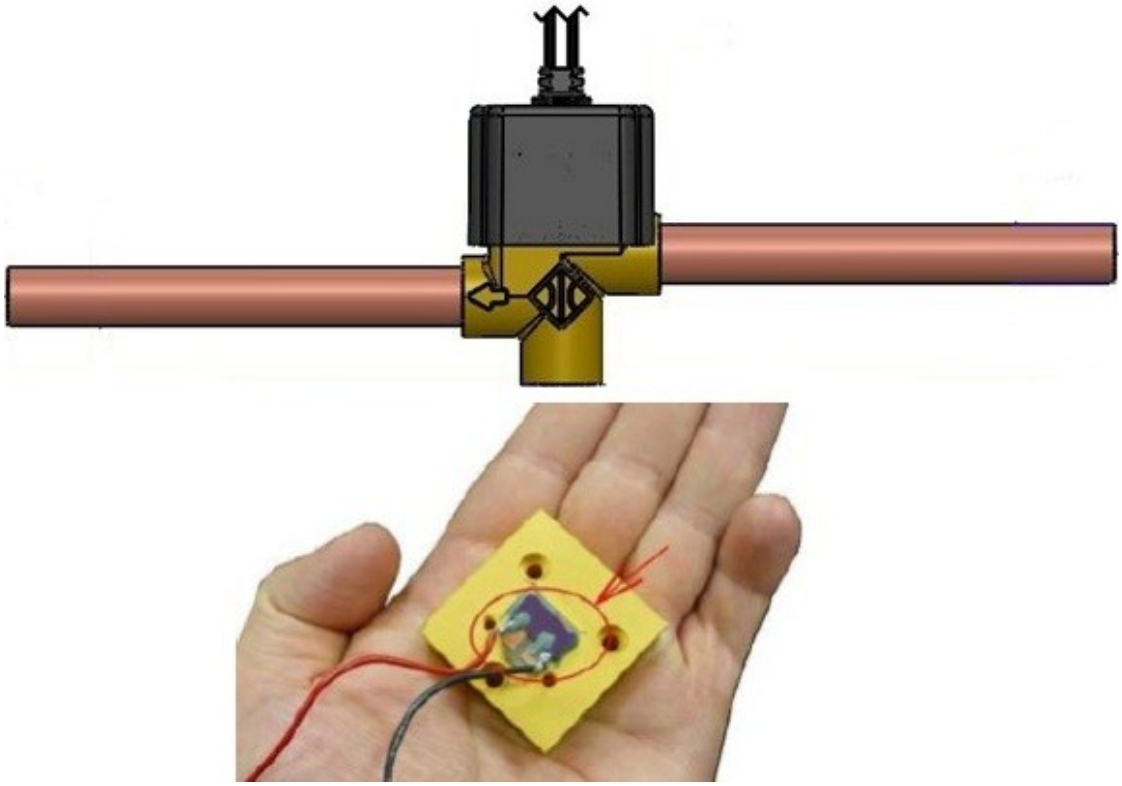

Figure 1-2 Prototype of Silicon Expansion Valve [6]

These valves facilitate miniaturization, multiple component integration, programmed control action, sensitive response and the less wear and tear. The complete design and working for the SEV can be found in their publications ([6], [7]). As claimed by Microstaq, supermarket refrigeration systems that have replaced their Thermal Expansion Valves (TEVs) with SEVs have shown energy savings up to 20%. But the exact cause of power savings is still uncertain. This research work provides an explanation for the energy savings observed in the supermarket refrigeration system retrofitted with the Silicon Expansion Valves.

With supermarkets being highly energy intensive buildings, improving the efficiency of the supermarket refrigeration systems will have serious energy saving

implications. To achieve superior efficiency, an engineer has to focus on improved design of system components and implementation of advanced control strategies. But prior to bring control schemes into practice, a nonlinear system model is a necessary requirement. The dynamic models should accurately capture the heat transfer and mass flow characteristics of the refrigeration system. This thesis makes contribution at both fronts. Firstly, the dynamic modeling of a three-evaporator supermarket refrigeration system is carried out. The simulation models are validated by experimental tests conducted on a commercial Hussmann supermarket open door display case. The experimental system is fitted with the MEMS based Silicon Expansion Valves (SEVs). Subsequently, an advanced cascaded controller is designed for the supermarket refrigeration unit. The MEMS based valves are controlled using the cascaded control strategy and the commercial Microstaq Superheat Controller (SHC). The experimental results reveal that the use of SEVs lead to significant efficiency gains over the mechanical Thermal Expansion Valves (TEVs). This thesis makes contribution in determining the cause of potential energy savings with the use of MEMS valves. It also details that the use of advanced cascaded control technique can lead to further improvement in efficiency of the supermarket refrigeration system as compared to the commercially available MS Superheat Controller and the mechanical valves.

1.1 Background

An ideal vapor compression cycle consists of four components as shown in Figure 1-3. These are the compressor, condenser, expansion valve and an evaporator.

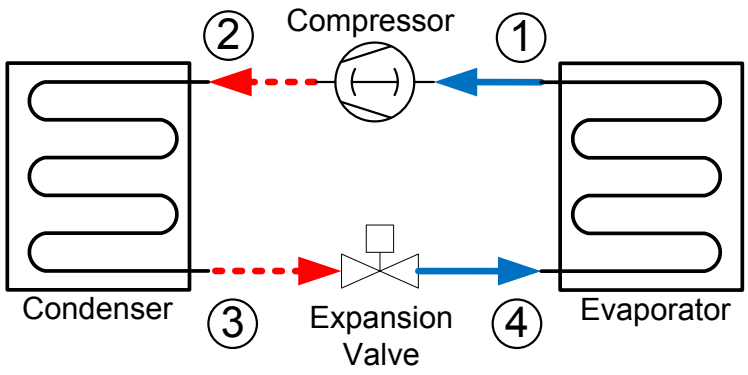

Figure 1-3 Ideal Vapor Compression Cycle [34]

The ideal vapor compression typically involves four processes: a) isentropic compression (state 1 to state 2), b) isobaric condensation (state 2 to state 3), c) isenthalpic expansion (state 3 to state 4), and isobaric evaporation (state 4 to state 1). The compressor pumps superheated refrigerant into the condenser, where it rejects heat, changes phase, and becomes a sub-cooled liquid. The liquid is throttled through the expansion valve where its pressure decreases. The refrigerant is a two-phase fluid at the evaporator entry. In the evaporator, it absorbs heat and becomes superheated where it then enters the compressor. The operation of this cycle can be represented by a Pressure-Enthalpy diagram as given in Figure 1-4. (Used with permission from the author [34]).

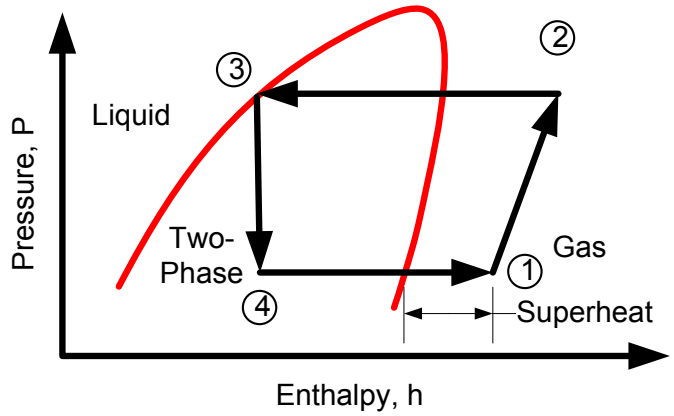

Figure 1-4 P-h Diagram of a Vapor Compression System [34]

Multi-evaporator systems are used both in residential and commercial buildings such as supermarkets, multiplexes, pharmaceutical industries, where different zones have different cooling requirements. Especially in supermarkets, different products such as fresh vegetables, dairy products, meat, frozen food etc. are stored in open and close door display cases, storage refrigerators and walk-in-coolers, based on different temperature needs of the product. Such an application increases the complexity of a vapor compression system. In a typical supermarket, there are multi-compressor racks and multi-fan condensers. Usually these equipments are located in a remote machine room or at the building roof. From the condensers the liquid-state refrigerant is distributed to the open door or the glass door display cabinets through a piping network. The advantage of using multiple compressors in parallel is that it can provide a means of capacity control [3]. The compressors can be selected and cycled to meet different refrigerant load requirements.

1.2 Literature Review

The mathematical modeling of the HVAC components has been a topic of interest for the researchers for several decades. Once a mathematical model of the system is determined, it eases the implementation of different control strategies for optimization and control of system components. A number of dynamic models for air-conditioners/refrigeration systems, validated by experiment are available in the literature. Bendapudi and Braun [8], provided literature review of the notable research work in this area. They have reported that the major task in the mathematical modeling of the refrigeration system is the modeling of the heat exchangers. Wedekind and Stoecker [9] were among the first persons to study transient behavior of the flow, in an evaporator. Wedekind later published his research on the transient behavior of a two-phase flow using the mean void fraction model [10]. His contribution led to the development of moving boundary methods, for modeling heat exchangers. Grald and MacArthur [11] used the moving boundary refrigerant model to present the transient interactions in one-dimensional two phase-flows. They used this technique to predict the temperature profile along the heat exchanger wall. Dhar [12] was among the first researchers to give a complete model of all the vapor compression components. In his doctoral thesis he modeled a window-air conditioner based on the first principles of the moving boundary approach. Chi and Didion [13] presented a lumped parameter approach to model an air-to air heat pump. Their paper is one of the few works that includes the transient form of momentum equation. Gruhle and Isermann [14] gave a theoretical model for an evaporator with complete equations for the expansion valves,

the compressor and the superheater. Their work also highlights the design of a superheat controller which is one of the major concerns of the HVAC industry. Later, Willatzen, Pettit and Ploug-Sørensen [15] developed sub-critical air conditioning systems models using the lumped-parameter, moving boundary approach. Rasmussen and Alleyne ([16]-[17]), carried extensive research in this area and validated the mathematical models with experiments. In their publication [18], they developed reduced order mathematical model, which sufficiently captures the major dynamics of the system without any significant loss of accuracy. Wei-Jiang and Chun-Lu [19] presented a time-varying void fraction approach to improve the robustness of existing moving boundary models under larger disturbances. Their work laid the foundation of capturing system dynamics in large transient periods like the start-up and the shutdown. Another approach which is in practice for the modeling of vapor compression systems is the Finite Control Volume (FCV) method. This technique accurately captures the transient behavior of the system parameters but is more simulation intensive. Abhishek Gupta [20] carried out extensive modeling using the FCV technique in his MS thesis at Texas A&M University. Later, Balakrishna Ayaagari [21] used the FCV approach to capture the system transients during the start-up and shut-down of the compressor. He validated the models on a 3-ton residential air conditioning system. The Finite Control Volume approach seeks to capture the salient dynamics of the system in more detail as compared to the Moving Boundary Approach which captures only the dominant dynamics of the vapor compression system. However the Moving Boundary Approach is more popular in

developing control techniques as it is less simulation intensive as compared to the Finite Control Volume method ([22], [23]).

To date, almost all relevant model development work, either the Moving Boundary or the Finite Control Volume focuses on one-evaporator system. In a multi-evaporator system, the evaporators are connected in parallel, and the dynamics of each evaporator influences the other one. Such behavior increases the complexity and difficulty in the mathematical modeling of the system. There are only a limited number of studies on modeling and control of such multi-evaporator supermarket refrigeration systems. Wu, Xingxi and Shimming [24] modeled a three evaporator air conditioner system by creating a sub-model of each evaporator. They also provide a self-tuning fuzzy logic algorithm to control the individual expansion valves of the three evaporators. However, their modeling approach is not validated by the experimental apparatus or when the system is subjected to external disturbances. For the open door display cases in the supermarkets, the refrigeration load is particularly large due to the cold air spillage from the cabinets. Ge and Tassour [25] presented that the cold air spillage is a function of open design of the cabinets. Tahir and Bansal [26] compared the performance of electronic expansion valves and the mechanical expansion valves on a supermarket refrigeration system. Their field tests show that the use of electronic valves significantly improves the air curtain strength of an open display case, reduce the frost formation and significantly improves the cabinet temperature.

For decades, mathematical modeling of the vapor compression systems and advanced control strategies for superheat regulation is in demand for the researchers.

However, as discussed earlier the dynamic modeling of multi-evaporator system increases the modeling complexity and only a limited number of publications are available. This thesis focuses on the dynamic modeling of a three-evaporator supermarket refrigeration system. A novel methodology of the modeling parallel evaporators which do not have a discharge valve at the outlet is discussed. Furthermore, experiments are conducted to investigate the cause of potential energy savings with the use of MEMS based Silicon Expansion Valves (SEVs) as compared to the Thermal Expansion Valves (TEVs). The research objectives and the corresponding tasks are mentioned in more detail in the next section.

1.3 Research Objectives and Tasks

The objective of this research is to validate the superior performance of the MEMS based SEVs on a commercial supermarket refrigeration unit as claimed Microstaq. The aim is to provide explanation for the potential energy savings derived in the supermarket refrigeration systems which are retrofitted with Microstaq Silicon Expansion Valves and their superheat controller.

These objectives are achieved by completing the following tasks 1) Mathematical modeling of a multi-evaporator supermarket refrigeration system was carried out and the simulation results were validated with the experimental setup. The dynamic models were validated by a three-evaporator supermarket open door display cabinet. The modeling approach proposed in this research can be generalized for any number of evaporators in a vapor compression cycle. 2) Experimental tests were performed to compare the

performance of thermal expansion valves with the MEMS based Silicon Expansion Valves which were controlled by the Microstaq SHC and the advanced cascaded controller. The comparison of the performance for the three actuating mechanisms was based on the superheat regulation, cooling and power consumption of the system and the COP of the system.

1.4 Organization of Thesis

The remainder of this thesis is organized as follows: Section 2 gives the details of each of the component of the experimental system which is used for the validation of the dynamic models. It also gives details about the various sensors and the Data Acquisition System which is used for doing the experiments. Section 3 describes the approach used for the modeling of multiple evaporators. The governing equations for the compressor and the valve models are also given in this section. Section 4 provides the simulation and the validation results. Section 5 talks about the design of the cascaded control and comparison of the performance of this controller with the mechanical valves and the commercial controller. Section 6 gives the final discussion, conclusion and the scope of future work.

2. EXPERIMENTAL SYSTEM

The experimental system used in this research is the Hussmann commercial refrigeration unit Excel B3XC-LEP. It is a three evaporator supermarket open door display cabinet as shown in Figure 2-1.

Figure 2-1 Hussmann Excel B3XC-LEP, Supermarket Open Door Display Cabinet

The three evaporators are connected to a single compressor and a condenser with the receiver at the outlet. The evaporators are air cooled, finned tube heat exchangers.

The condenser is a water-cooled, plate type heat exchanger. The system is fitted with both the Silicon Expansion Valves and the Thermal Expansion Valves using the by-pass valves. A total of 11 thermocouples have been installed. Three of them are placed on the liquid line to measure the inlet temperature of the refrigerant to the evaporators. Six of them measure the air inlet and outlet temperatures for the evaporator. The other two measure the temperature on the water line of the condenser. Three pressure sensors are installed on the low side and one on the high side. There are three mass-flow sensors which measure the inlet mass flow rate of the refrigerant to the evaporators. The system is also fitted with three commercial Microstaq Superheat Controllers at the outlet of each evaporator. The system features variable air flow and variable refrigerant mass flow, using the SEVs. The unit runs on R404 A as the refrigerant. A complete schematic of the system layout is given in Figure 2-2.

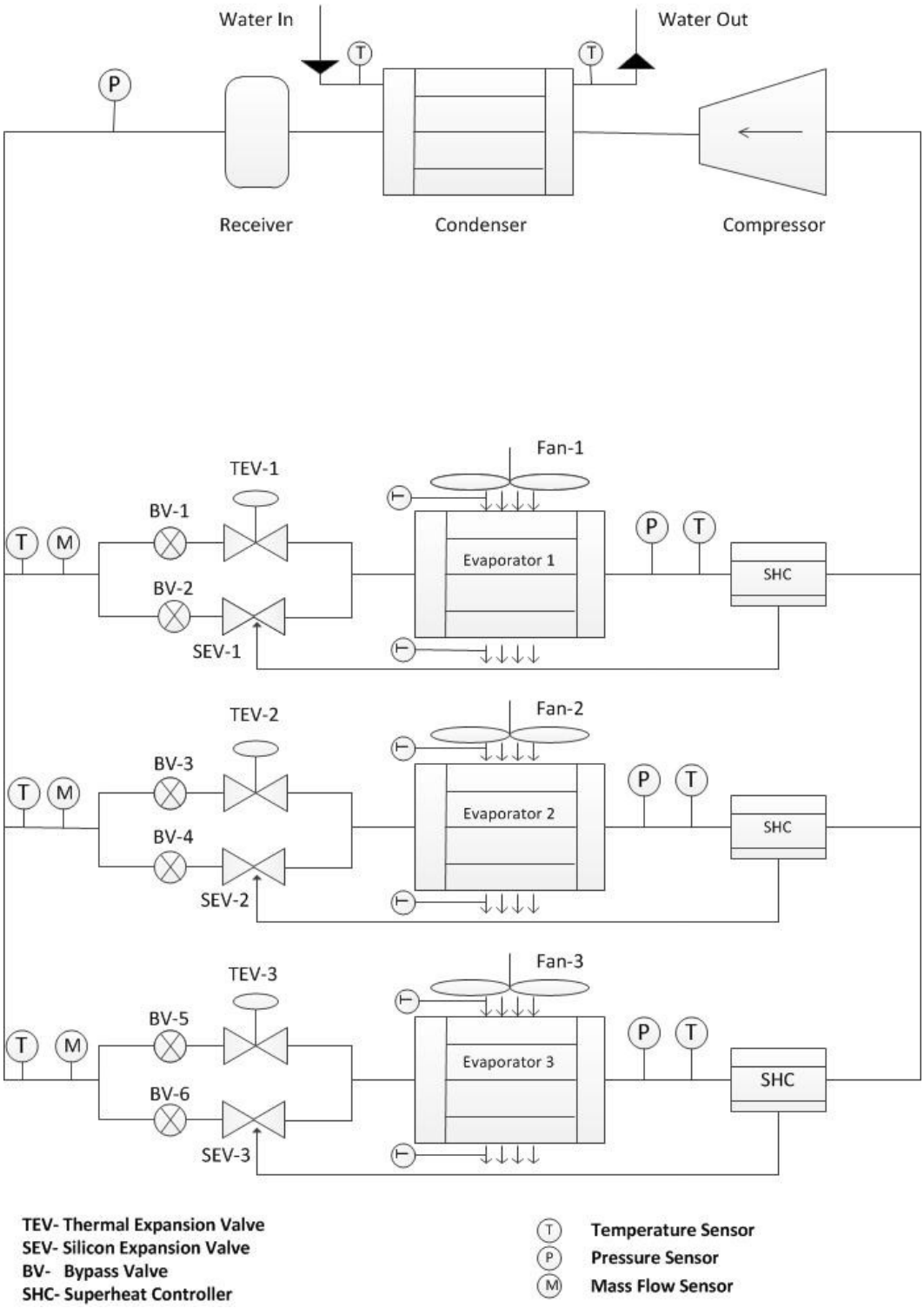

Figure 2-2 Schematic of the System

All piping is of copper tubing while the evaporator coils are made of aluminum. The liquid line is ¼'' copper tube while the suction line is 1'' copper tube. The sensors are fixed to the system by using Swagelok brass and stainless steel compression fittings.

2.1 Details of System Components

2.1.1 Compressor

The compressor installed on this system is single speed reciprocating type compressor manufactured by Ingersoll Rand Inc as shown in Figure 2-3. It is powered by a three phase AC voltage of 208/230 V at 60 Hz. At the nominal voltage it has a speed of 1750 rpm.

Figure 2-3 Compressor

2.1.2 Condenser

The condenser is a water cooled plate type heat exchanger manufactured by Swep International Inc. as shown in the Figure 2-4. It is a brazed type plate heat exchanger having 80 parallel plates. It features single pass and counter current flow. The water to the condenser is supplied through the hose using the water tap at the lab. The water is supplied at a rate of 5 gpm.

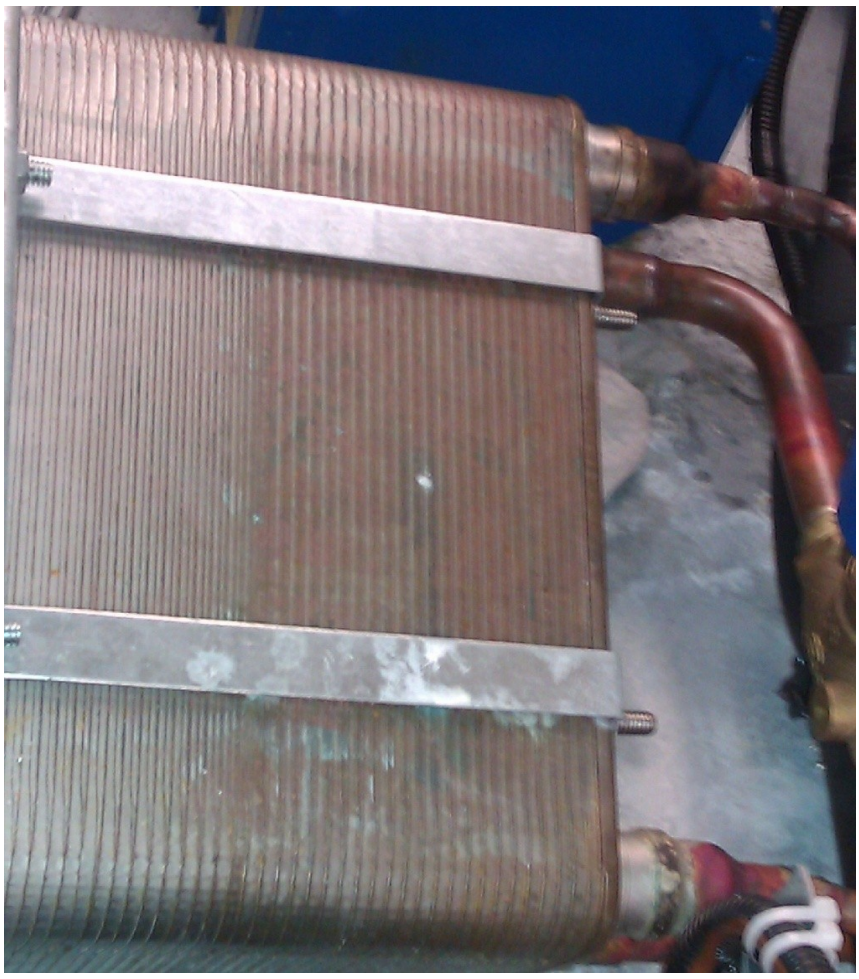

Figure 2-4 Condenser

2.1.3 Liquid Receiver

The system features a refrigerant receiver at the outlet of the condenser, manufactured by Refrigeration Specialties Group, as given in Figure 2-5. It has a design pressure of 500 psi (4335 kPa). The purpose of the receiver is to ensure saturated liquid refrigerant to the expansion valves.

Figure 2-5 Liquid Receiver

2.1.4 Expansion Valves

Both the thermal expansion valves and the silicon expansion valves are installed in the system. Details of the MEMS based Silicon Expansion Valves is provided earlier. The by-pass valves are used to run the unit either on TEVs or the SEVs. Figure 2-6 through Figure 2-8 shows the TEV, the SEV and a by-pass valve.

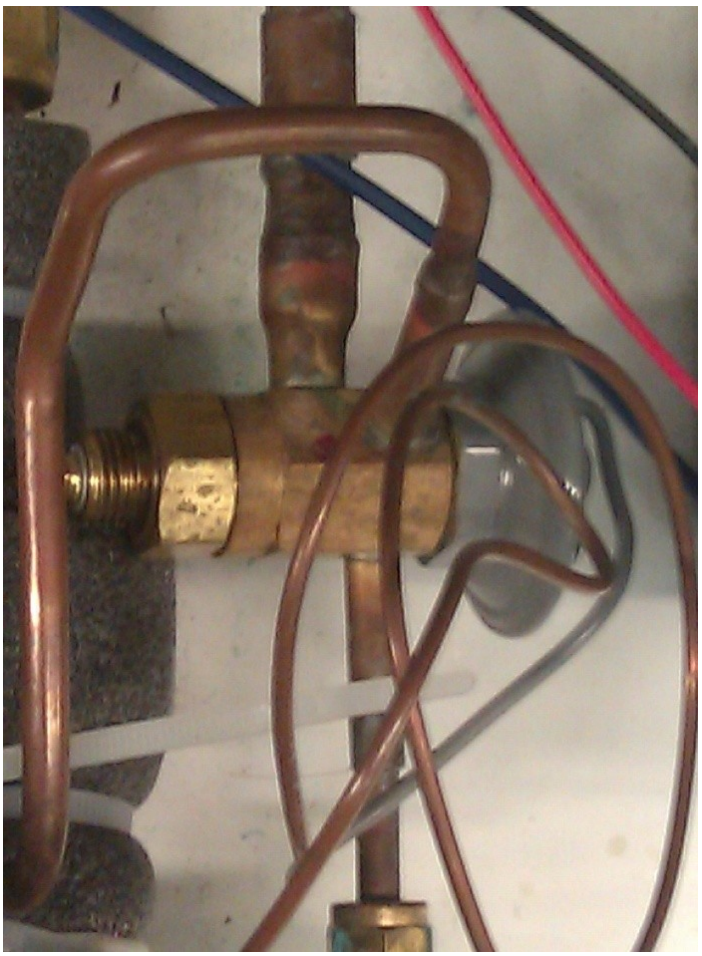

Figure 2-6 Thermal Expansion Valve

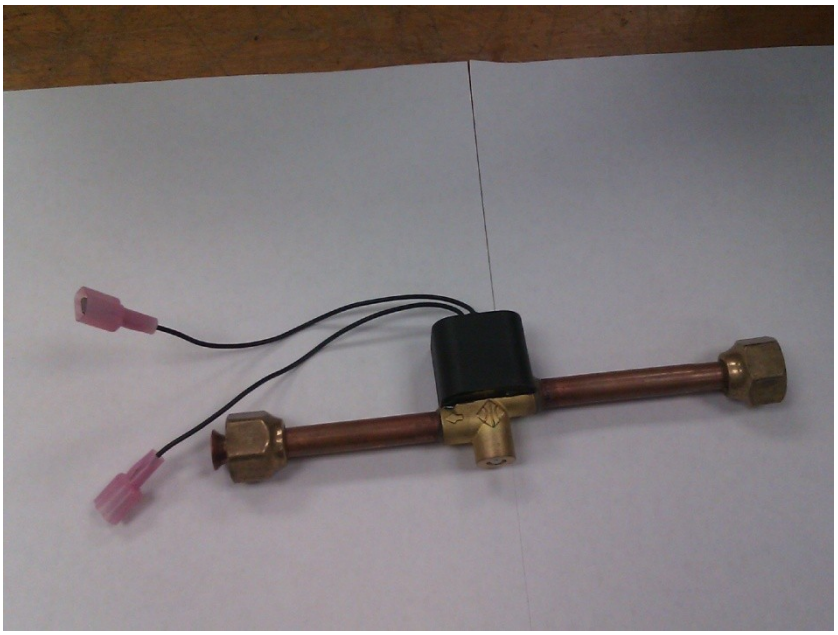

Figure 2-7 Silicon Expansion Valve

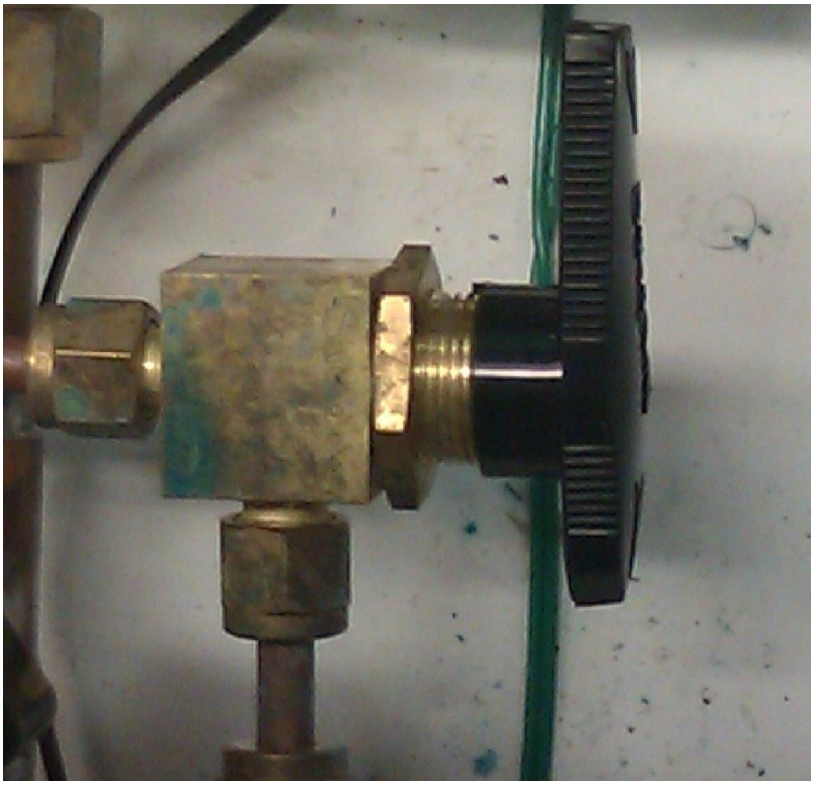

Figure 2-8 Bypass Valve

2.1.5 Superheat Controller

There are three commercial superheat controllers (SHC) developed by Microstaq installed at the outlet of each evaporator. The controllers have inbuilt pressure and temperature sensors. The controller is powered by 24 V AC supply using a transformer box. The controller is connected to the computer with a USB connector through a USB to RS422 convertor. The controllers are activated using Graphical User Interface software v2.9 developed by Microstaq. Figure 2-9 through Figure 2-11 shows the Microstaq SHC, the graphical user interface and the USB to RS-422 converter respectively.

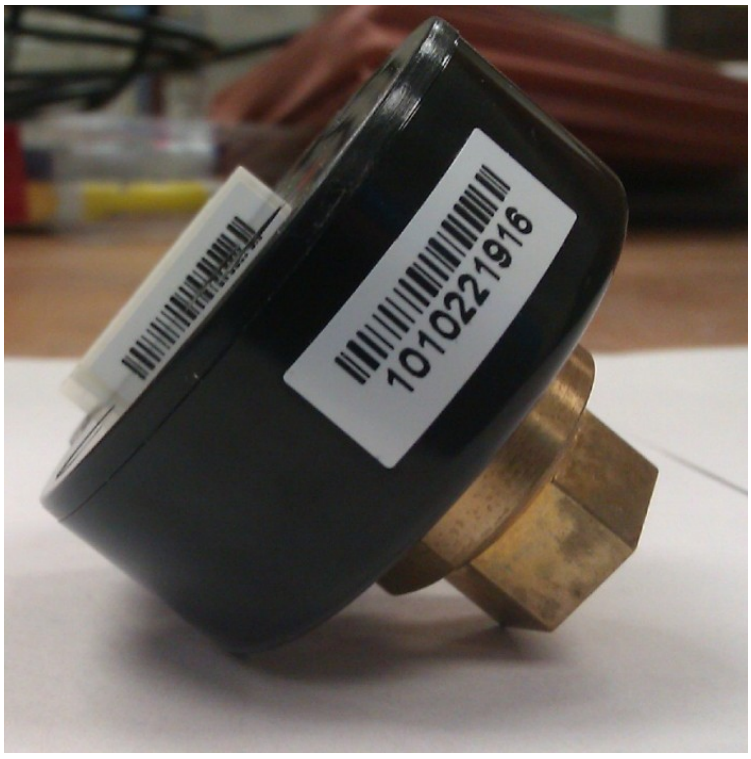

Figure 2-9 Superheat Controller

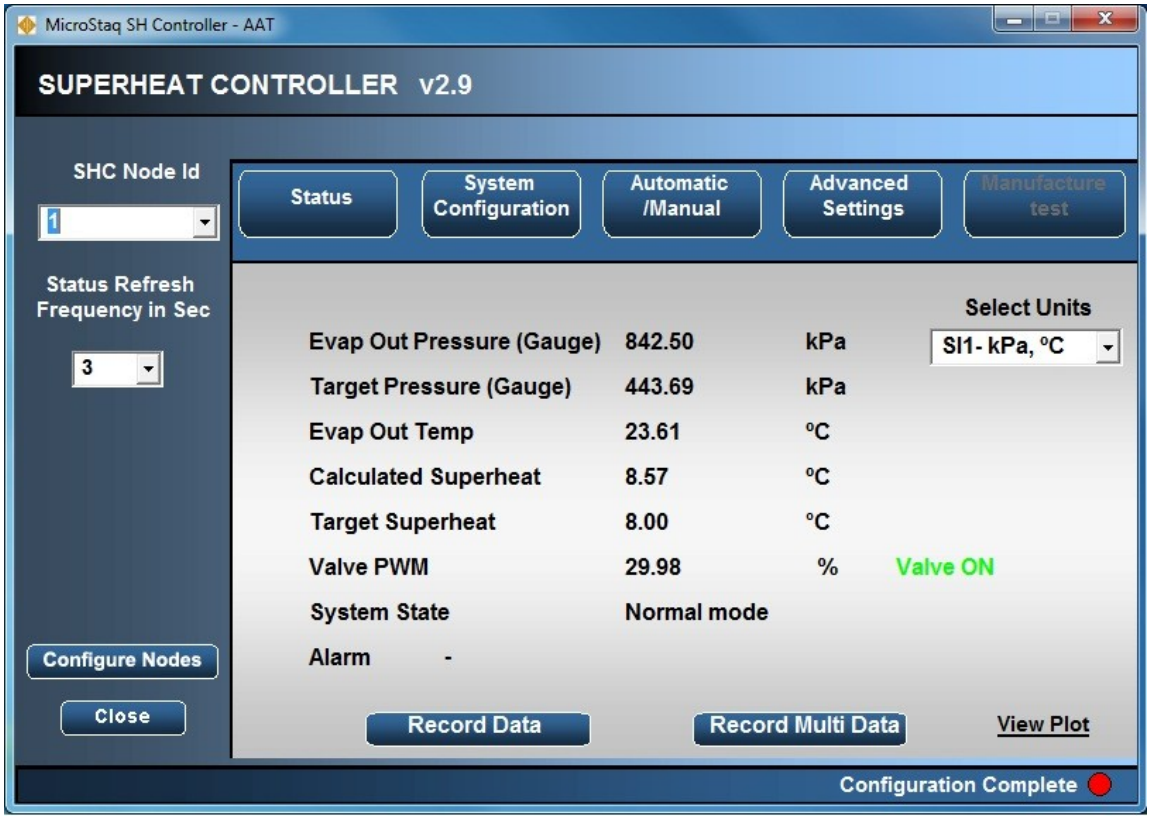

Figure 2-10 Microstaq Superheat Controller Graphical User Interface (GUI)

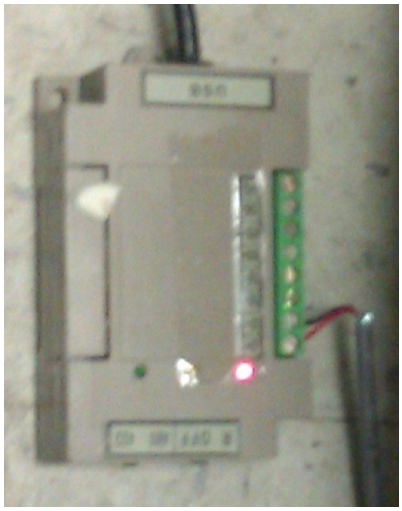

Figure 2-11 USB to RS422 Converter

2.1.6 Evaporators

The system evaporators are finned tube heat exchangers as shown in Figure 2-12. The evaporator coil consists of two parallel aluminum tubes, through which the refrigerant flows. There are a total of 120 plate type fins.

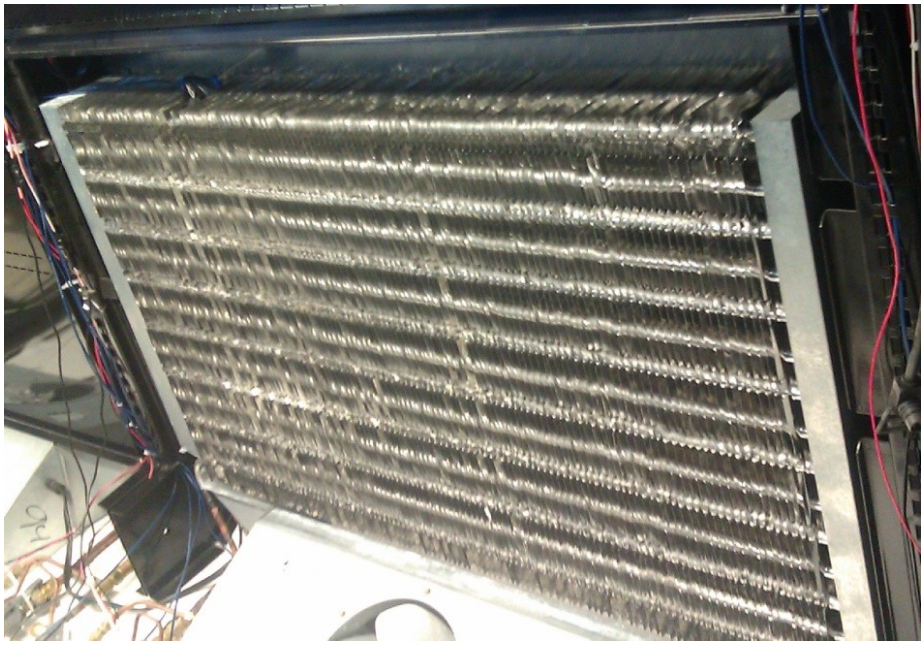

Figure 2-12 Evaporator

2.1.7 Evaporator Fans

The unit features three fans to which are used to circulate air through the unit as depicted in Figure 2-13. The fans blow the air through the evaporator coils, which in process gets cooler and then again circulated within the system. The fans are powered by variable speed motor. The speed of the fans is controlled using the Smart Fan Speed Control Box.

Figure 2-13 Evaporator Fan

2.2 Details of Sensors

2.2.1 Thermocouple

The thermocouple is a T-type thermocouple made by Omega Inc., as shown in Figure 2-14. They are used to measure the refrigerant temperature, the air temperature on the evaporator side and the water temperature on the condenser side. They send 0-5 VDC signal output.

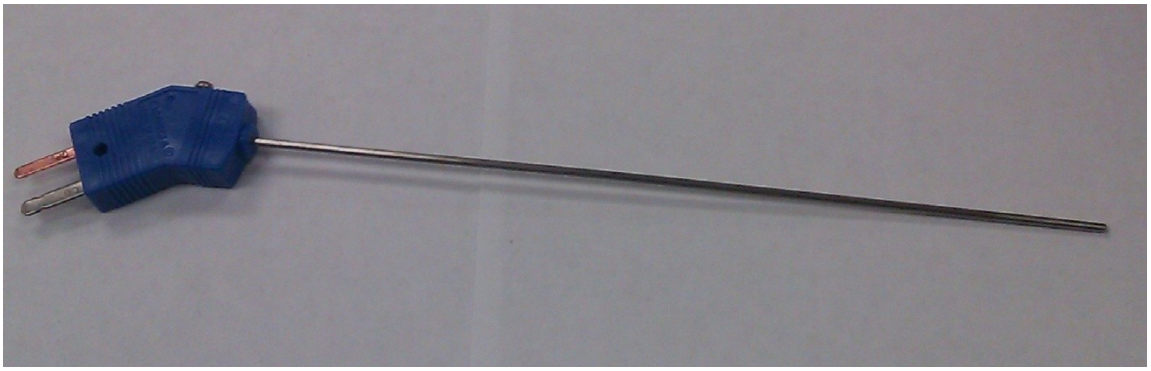

Figure 2-14 Thermocouple

2.2.2 Pressure Sensor

The pressure transducers are manufactured by Omega Inc., as shown in Figure 2-15. They are used to measure the liquid line pressure for the three evaporators and the suction line pressure. The pressure sensors are powered by a 9 V DC supply. They send out a 0-5 VDC signal output.

Figure 2-15 Pressure Sensor

2.2.3 Mass Flow Sensor

The mass flow sensors are manufactured by McMillan Inc., as shown in the Figure 2-16. They are used to measure the refrigerant flow to the evaporators. They are powered by 24 V DC supply and send out a 0-5 VDC signal output.

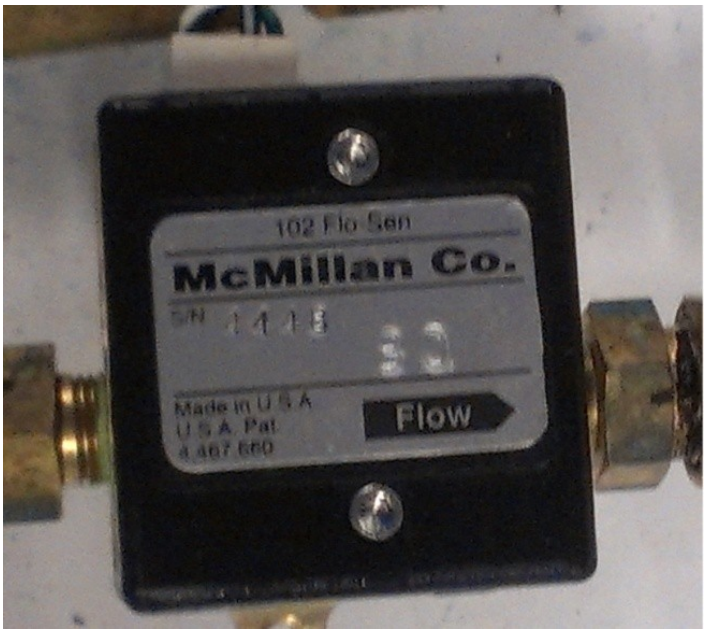

Figure 2-16 Mass Flow Sensor

2.2.4 Power Transducer

The power transducer is used to measure the compressor and the lights. It is manufactured by CR Magnetics. It is powered by a 9 V DC supply and measures the power by measuring the AC current and voltage to the system. It gives a 0-5 V DC output. Figure 2-17 shows the power transducer used on the system.

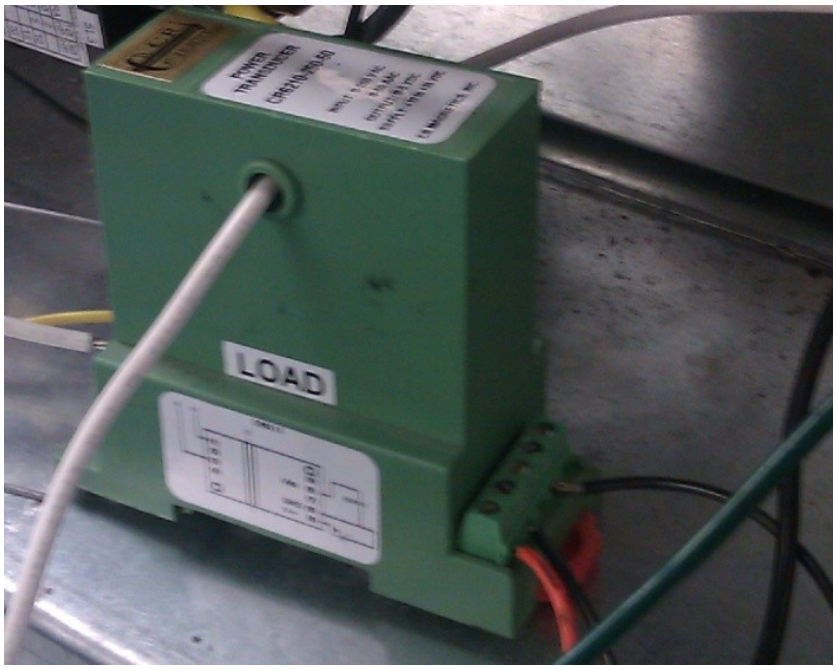

Figure 2-17 Power Transducer

Table 2-1 gives the details of each of the components and the sensors used in the system.

Table 2-1 List of the Components

Part	Manufacturer	Part No.	Quantity
Compressor	Ingersoll Rand	IR2CO278SK	1
Condenser	Swep Inc.	B10THx80	1
Liquid Receiver	Refrigeration Specialties Group	3389	1
Thermal Expansion Valve	Sporlan	Unknown	3
Silicon Expansion Valve	Microstaq	SH15K2	3
By-Pass Valve	Swagelok	B-43S4	6
Superheat Controller	Microstaq	1010221916	3
Evaporator Fans	Hussmann	4410546	3
Fan Control Box	Control Resources	180V-800E	1
Thermocouple	Omega	GTMQSS-062U-6	11
Pressure Transducer	Omega	PX309-300G5V	4
Mass Flow Sensor	McMillan	Model 102	3
Power Transducer	CR Magnetics	CR6210-250-50	1
USB-RS422 Converter	Donated by Microstaq	Unknown	1

2.3 Data Acquisition

2.3.1 Ni-Daq System

The Data Acquisition Board used for recording data and real time control of the hardware is carried out by National Instruments, compact device cDAQ-9178. It is connected to the DAQ PC through the USB connection and is powered by a 120 VAC supply. Three different NI modules are used for Analog Input (NI-9201, 8 channels), Analog Output (NI-9263, 8 channels) and the thermocouples (NI-9213, 16 channels). Analog output signals are used to control the evaporator fan speed and the valve openings. The Analog input signals measure the pressures, mass flow rates and the

power. The temperatures logging is done using the thermocouple module. The modules are attached externally to the cDAQ board as shown in Figure 2-18.

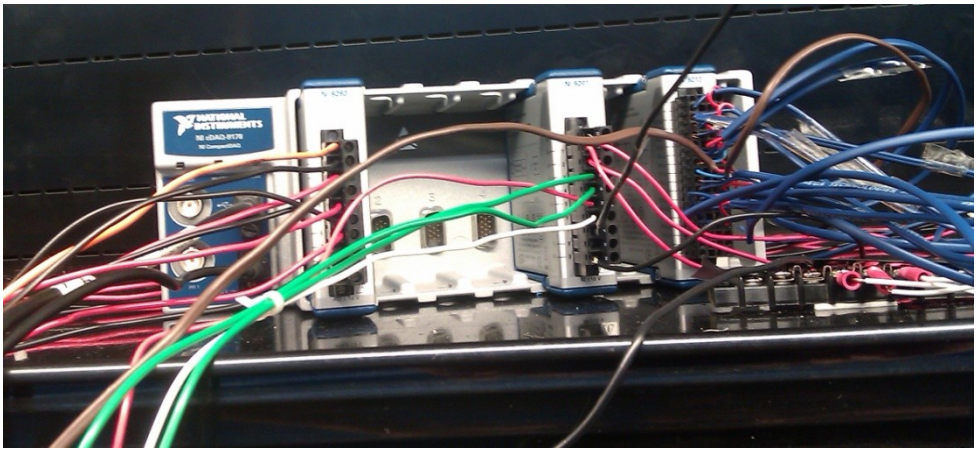

Figure 2-18 NI-cDAQ 9172 and Modules

Figure 2-19 below shows the DAQ-PC which is connected through a USB port to the NI-cDAQ board.

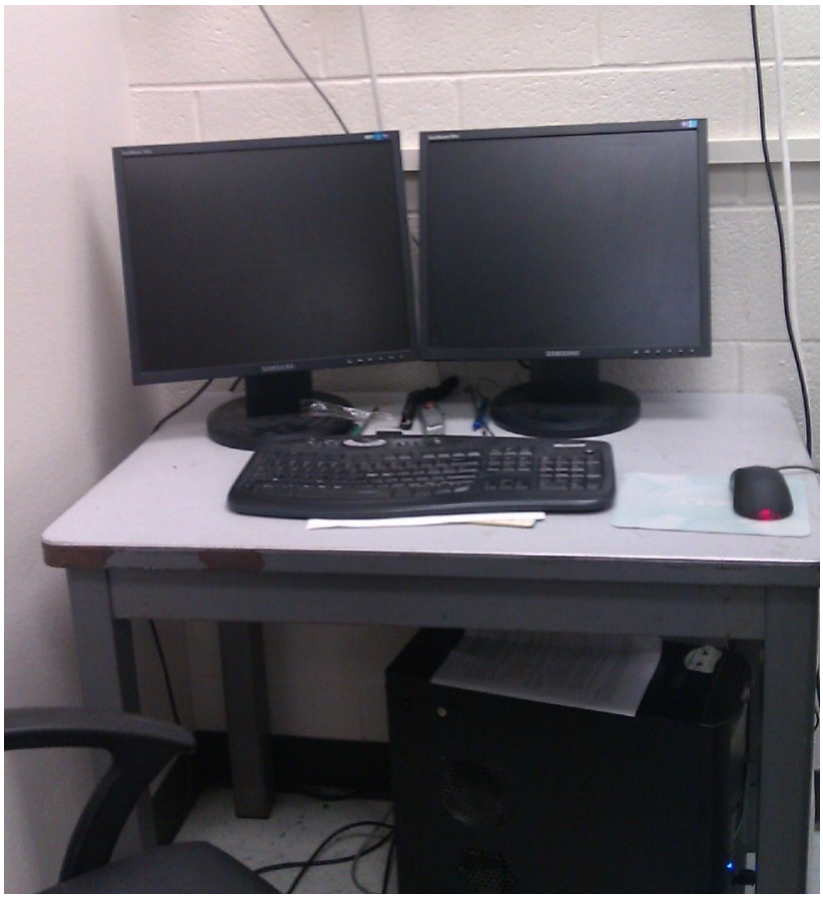

Figure 2-19 The DAQ PC

2.3.2 Software

The data logging is done by Labview 2011 (32 bit) and Quarc 2.2, a software package developed by Quanser. A Labview VI was first created for the real time data measurement and control of the hardware using the NI- cDAQ board. Quarc 2.2 was then used to create a network server connection between the LABVIEW and SIMULINK. Quarc allows Simulink to be the user interface. It features additional blocks like “Connection Server”, which was used to connect Labview and Simulink. The signals can be sent from Simulink and received by Labview and vice versa by creating a

Network Server connection. Figure 2-20 - Figure 2-22 shows the Labview VI and the Quarc/Simulink interface.

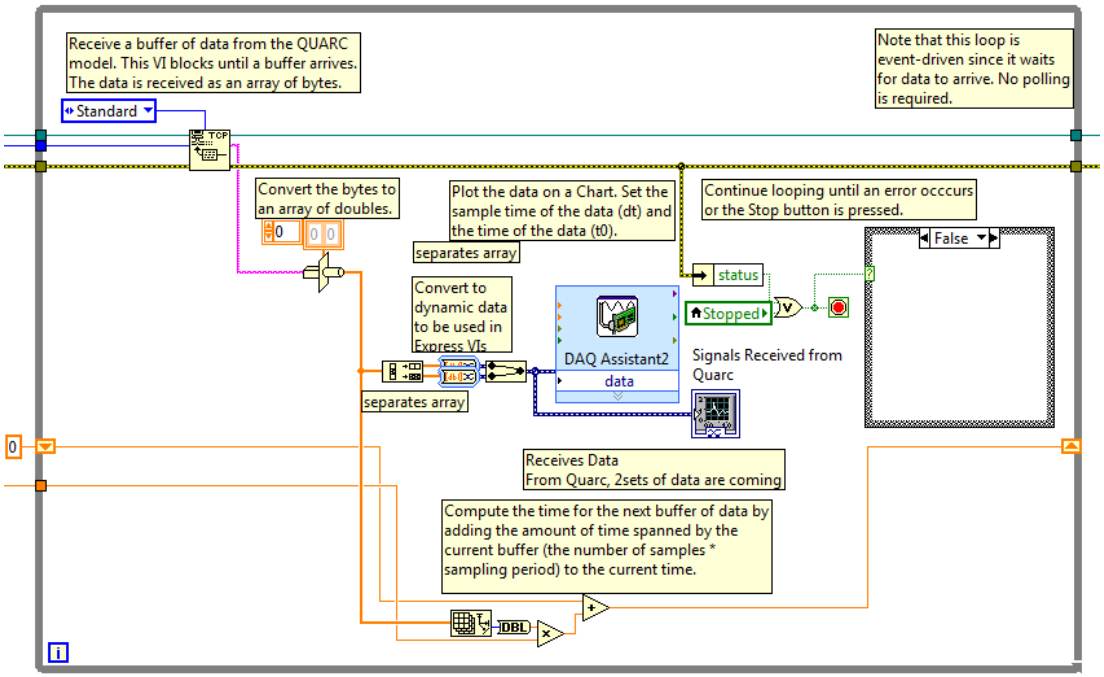

Figure 2-20 Labview VI for Receiving Signals from Quarc/Simulink

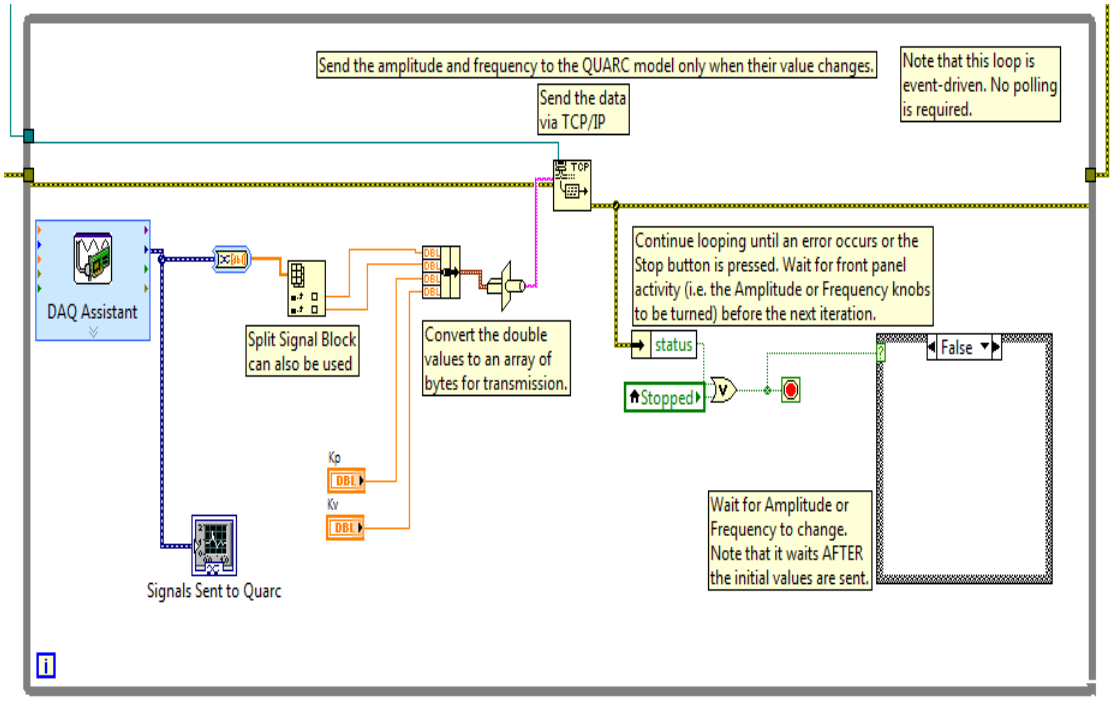

Figure 2-21 Labview VI for Sending Signals to Quarc/Simulink

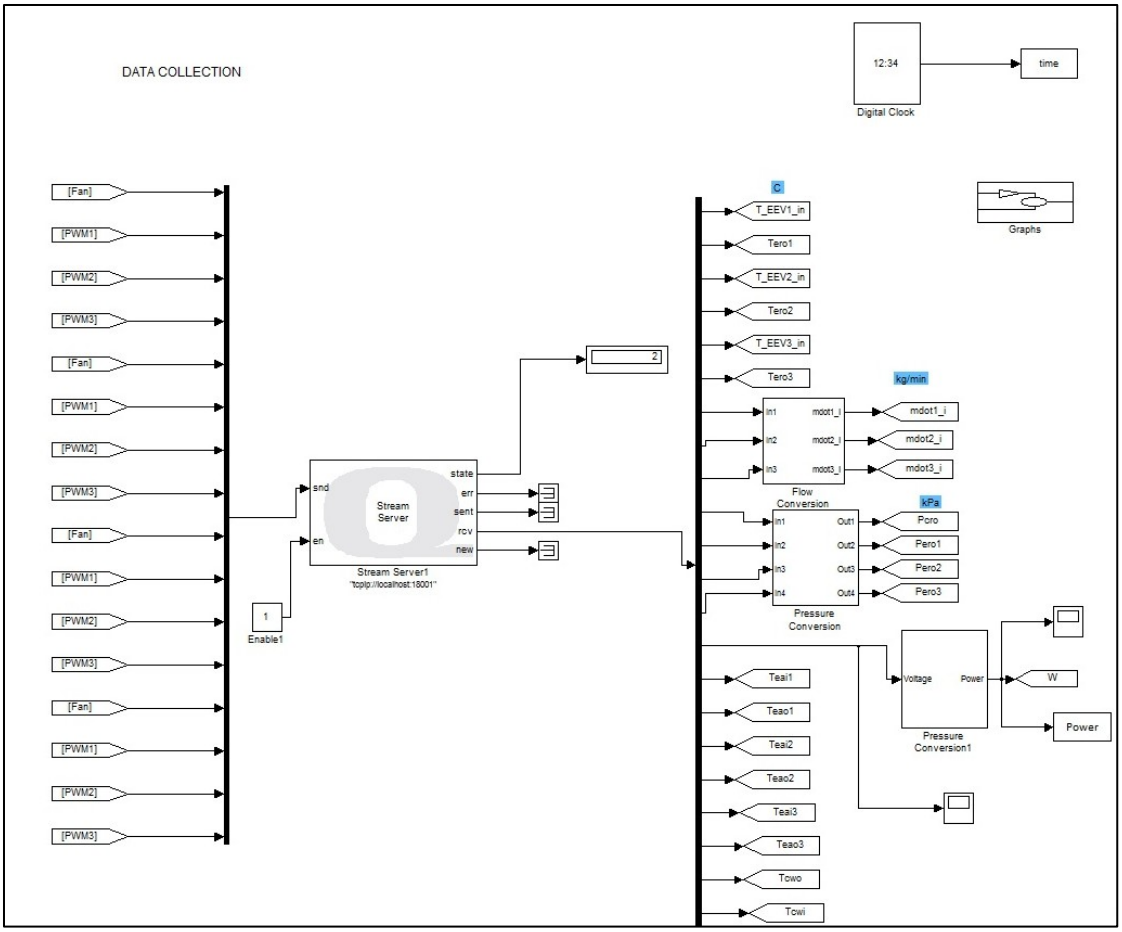

Figure 2-22 Quarc/Simulink Interface

All parameters including controller gains, data logging and real time control of the hardware is carried out through this interface.

3. MODELING APPROACH

A standard vapor compression system model is constructed by appropriately integrating models for each of the individual component models that compose the cycle: the compressor, the three evaporators, three expansion valves and the condenser. The dynamic models of individual components are created in Matlab–Simulink R2011b. The mathematical modeling of the condenser was not done in this study. The primary focus is on the dynamics of the three evaporators that determine evaporator outlet pressures and the enthalpies. Mass flow devices such as compressors and valves utilize inlet and outlet pressures to determine mass flow rates. Outlet fluid enthalpy is determined by each component model and supplied as an input to subsequent component models. The condenser pressure and the outlet enthalpy were directly used from the experimental values, to complete the model integration.

3.1 Modeling Assumptions

Dynamic modeling of the vapor compression components is quite complex due to high order and non-linearity in the mathematical equations. So there have been some assumptions made which simplify the development of the governing equations. Firstly, the dynamics of the valves and the compressor are assumed to change at a much faster time scale as compared to the heat exchangers. Henceforth, expansion valves and the compressor are modeled as static models while the evaporator is modeled based on dynamic relationships. Secondly, the heat exchanger is assumed to be a one-

dimensional, horizontal long tube. In reality, the refrigerant flow inside the coils of the evaporator is a three-dimensional, turbulent flow. This effect is taken care of by choosing appropriate air side and the refrigerant side heat transfer coefficients. Thirdly, the pressure drop across the length of the tube of the evaporator due to viscous flow is assumed to be negligible. This assumption simplifies the model by excluding the governing equations of the conservation of momentum across the length of the heat exchanger. Lastly, the flow of refrigerant through the expansion valve is assumed to be isenthalpic.

3.2 Evaporator Modeling

Previous literature review as given in Section 1, show that the bulk of dynamics of the heat exchanger is the two-phase flow of the refrigerant [8]. In this thesis, the modeling procedure for the evaporator follows the lines of previous work, as discussed in Section1. The standard moving boundary, lumped parameter approach is used to model the three evaporators ([13], [16], [19], [22], [23]) with time-invariant mean void fraction. This methodology seeks to capture the salient dynamics of the system by assuming a time-varying boundary between different fluid phase regions (superheated, two-phase or subcooled) and constructs separate control volumes which "lump" the distributed parameters for each of these regions. Figure 3-1 (Used with permission from the author [16]) shows a MB evaporator model split into two control volumes: two-phase and superheated.

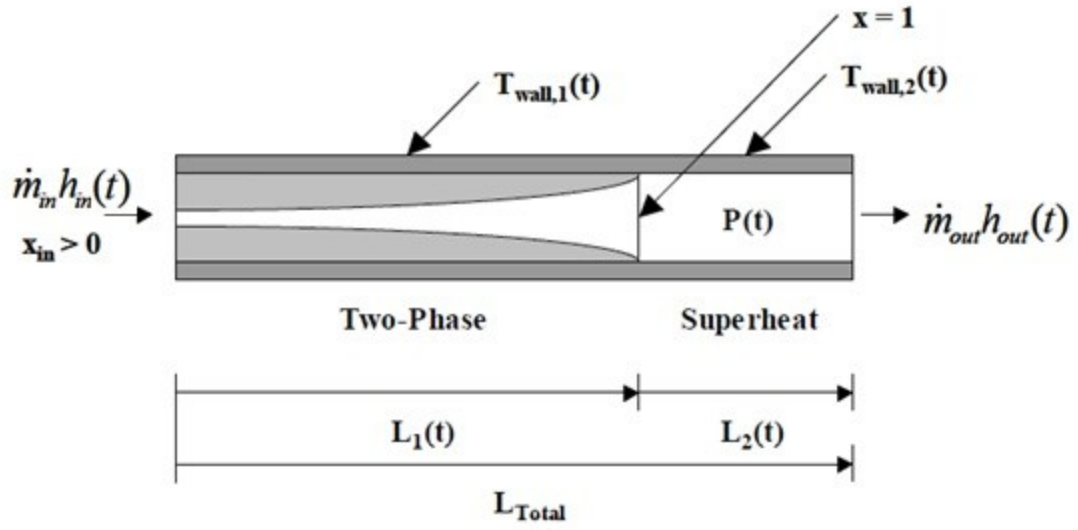

Figure 3-1 Moving Boundary Evaporator [16]

A general vapor compression system can be described by a system of differential-algebraic equations (DAEs) of the form as given in equation 1. In this form x represents the dynamic states, $\dot{x}$ is the associated time derivative vector and u is the external input vector. The vector $f(x,u)$ includes mass, energy and other system parameters which is the driving force for the dynamics of the system. The matrix $Z(x,u)$ include important variables which can be easily measured (like refrigerant pressure, temperature, etc.) and help facilitate simulation.

$$Z(x,u)\dot{x} = f(x,u) \tag{1}$$

For a single evaporator, conservation equations for refrigerant mass, energy, and wall energy can be applied to each of the control volumes and the governing equations for the heat exchanger can be derived in the form of state vector and external input vector as given in equations 2 and 3. The explicit time derivatives present in the

conservation equations are L_1 , the time variant length of the two phase region, P_e the refrigerant pressure in the evaporator, h_{out} the outlet enthalpy of the refrigerant and the wall temperatures in the two-phase and superheated regions of the evaporator, $T_{w,1}$ and $T_{w,2}$.

$$x = [L_1 \quad P_e \quad h_{out} \quad T_{wall,1} \quad T_{wall,2}] \tag{2}$$

$$u = [\dot{m}_{in} \quad \dot{m}_{out} \quad h_{in} \quad T_{air,in} \quad \dot{m}_{air}] \tag{3}$$

As stated earlier, the complete characteristics of the heat exchanger can be determined by the equations of conservation of refrigerant mass, energy and the wall energy. Earlier efforts have been made by the researchers to model multi-evaporators which have discharge valve at the outlet of each evaporator. In a system with discharge valve manifold, different evaporators operate at different pressures. The discharge valve at the outlet of each evaporator behaves like an isenthalpic expansion device, which brings down the pressure in each evaporator to that of an evaporator which has the least pressure or the compressor suction pressure. The discharge valves also ensure that there is no flow of refrigerant from one evaporator to the other. Rasmussen et al. [27] in their report to the Air Force Research Laboratory's (AFRL) modeled a three-evaporator system with discharge valves at the outlet of each evaporator. Component modeling was followed by system level integration. The heat exchangers were modeled by the standard moving boundary approach and the two discharge valves as the expansion devices. The system was integrated by feeding the outlet pressure and enthalpy from each evaporator to the discharge valves. The compressor suction pressure was used as input to the

discharge valve model for its outlet pressure. They have presented simulation results with transient external disturbances in their report to AFRL.

For a system with parallel evaporators without the discharge valves at the outlet, the complexity in integrating the components vastly increase. This is because the evaporators actually operate at pressures which are slightly different from each other. There is also the possibility of the refrigerant flowing from one evaporator to the other. In order to capture the accurate dynamics at the evaporators' outlet using the previous system level integration approaches, will involve the solver to solve the differential equations at very small discrete time steps. This makes the modeling very simulation intensive and not ideal for developing control algorithms.

In this research a novel approach is proposed to model multiple parallel evaporators which do not have discharge valves at the outlet. The governing equations for mass, energy and wall energy for all the heat exchangers can be combined together and solved simultaneously at discrete time steps. In this thesis, dynamic modeling of a three evaporator system without the discharge valves is done but the approach can be generalized for n-parallel evaporators. The conservation of refrigerant mass, energy and the wall energy equations for the three heat exchangers are combined together based on the two underlying assumptions.

- The rate of change of pressure should be same for each evaporator as shown in equation 4.

- The mass flow rate at the inlet of the compressor should be equal to the summation of the mass flow rates at the outlet of each evaporator as given in equation 5.

$$\dot{P}_e{}^1 = \dot{P}_e{}^2 = \dot{P}_e{}^3 \tag{4}$$

$$\dot{m}_{comp.} = \dot{m}_{out}{}^1 + \dot{m}_{out}{}^2 + \dot{m}_{out}{}^3 \tag{5}$$

Where, superscripts 1, 2, 3 refer to evaporators 1, 2 and 3 respectively and are subsequently used throughout this section.

Appendix A gives all the mathematical differential equations for the dynamic modeling of a three evaporator model. These governing equations of individual evaporators can be algebraically combined in the form given by $Z(x,u)\dot{x} = f(x,u)$ based on the above two assumptions to formulate a combined non-linear model for the three evaporators.

The corresponding new state vector x and a new input vector u are defined in equation 6 and equation 7 respectively.

$$x = [L_1{}^1 \quad P_e{}^1 \quad h_{out}{}^1 \quad T_{wall,1}{}^1 \quad T_{wall,2}{}^1 \; m_{out}{}^1 \tag{6}$$

$$L_1{}^2 \quad P_e{}^2 \quad h_{out}{}^2 \quad T_{wall,1}{}^2 \quad T_{wall,2}{}^2 \; m_{out}{}^2 \; L_1{}^3 \quad P_e{}^3 \quad h_{out}{}^3 \quad T_{wall,1}{}^3$$

$$u = [\dot{m}_{in}{}^1 \quad h_{in}{}^1 \quad T_{air,in}{}^1 \quad \dot{m}_{air}{}^1 \quad \dot{m}_{in}{}^2 \quad h_{in}{}^2 \quad T_{air,in}{}^2 \quad \dot{m}_{air}{}^2 \quad \dot{m}_{in}{}^3 \; h \tag{7}$$

$$T_{air,in}{}^3 \; \dot{m}_{air}{}^3 \; \dot{m}_{comp} \;]$$

The reader should note that the outlet mass flow rate for each evaporator is now one of the variables in the state vector and the mass flow rate to the compressor is a variable in the input state vector.

Another advantage of using this approach is that it can be generalized to model any number of parallel evaporators in a system, which do not feature discharge valves at the evaporator outlet. For an 'n-parallel evaporator system', the number of algebraic equations and total number of elements in the state vector will be $6n$. The Z matrix will be a square matrix of the order $6n\ x\ 6n$. The details of model start-up and the simulation results are given in Section 4.

Since, our dynamic model features a three evaporator system so the size of the matrix $Z(x,u)$ is a 18 x 18 matrix. The elements of the matrix $Z(x,u)$ are derived and presented in the Appendix. All the equations can now be reformulated and again be expressed in the form $Z(x,u)\dot{x} = f(x,u)$ as shown in equation 8.

$$
\begin{bmatrix}
z_{11} & z_{12} & z_{13} & 0 & 0 & z_{16} & 0 & 0 & 0 & 0 & 0 & 0 & 0 & 0 & 0 & 0 & 0 & 0 \\
z_{21} & z_{21} & z_{23} & 0 & 0 & z_{26} & 0 & 0 & 0 & 0 & 0 & 0 & 0 & 0 & 0 & 0 & 0 & 0 \\
z_{31} & z_{32} & z_{33} & 0 & 0 & z_{36} & 0 & 0 & 0 & 0 & 0 & 0 & 0 & 0 & 0 & 0 & 0 & 0 \\
z_{41} & 0 & 0 & z_{44} & 0 & 0 & 0 & 0 & 0 & 0 & 0 & 0 & 0 & 0 & 0 & 0 & 0 & 0 \\
z_{51} & 0 & 0 & 0 & z_{55} & 0 & 0 & 0 & 0 & 0 & 0 & 0 & 0 & 0 & 0 & 0 & 0 & 0 \\
0 & z_{62} & 0 & 0 & 0 & 0 & 0 & z_{68} & 0 & 0 & 0 & 0 & 0 & 0 & 0 & 0 & 0 & 0 \\
0 & 0 & 0 & 0 & 0 & 0 & z_{77} & z_{78} & z_{79} & 0 & 0 & z_{7\,12} & 0 & 0 & 0 & 0 & 0 & 0 \\
0 & 0 & 0 & 0 & 0 & 0 & z_{87} & z_{88} & z_{89} & 0 & 0 & z_{8\,12} & 0 & 0 & 0 & 0 & 0 & 0 \\
0 & 0 & 0 & 0 & 0 & 0 & z_{97} & z_{98} & z_{99} & 0 & 0 & z_{9\,12} & 0 & 0 & 0 & 0 & 0 & 0 \\
0 & 0 & 0 & 0 & 0 & 0 & z_{10\,7} & 0 & 0 & z_{10\,10} & 0 & 0 & 0 & 0 & 0 & 0 & 0 & 0 \\
0 & 0 & 0 & 0 & 0 & 0 & z_{11\,7} & 0 & 0 & 0 & z_{11\,11} & 0 & 0 & 0 & 0 & 0 & 0 & 0 \\
0 & 0 & 0 & 0 & 0 & 0 & 0 & 0 & 0 & 0 & 0 & 0 & z_{12\,13} & z_{12\,14} & z_{12\,15} & 0 & 0 & z_{12\,18} \\
0 & 0 & 0 & 0 & 0 & 0 & 0 & 0 & 0 & 0 & 0 & 0 & z_{13\,13} & z_{13\,14} & z_{13\,15} & 0 & 0 & z_{13\,18} \\
0 & 0 & 0 & 0 & 0 & 0 & 0 & 0 & 0 & 0 & 0 & 0 & z_{14\,13} & z_{14\,14} & z_{14\,15} & 0 & 0 & z_{14\,18} \\
0 & 0 & 0 & 0 & 0 & 0 & 0 & 0 & 0 & 0 & 0 & 0 & z_{15\,13} & 0 & 0 & z_{15\,16} & 0 & 0 \\
0 & 0 & 0 & 0 & 0 & 0 & 0 & 0 & 0 & 0 & 0 & 0 & z_{16\,13} & 0 & 0 & 0 & z_{16\,17} & 0 \\
0 & 0 & 0 & 0 & 0 & 0 & 0 & z_{17\,8} & 0 & 0 & 0 & 0 & 0 & z_{17\,14} & 0 & 0 & 0 & 0 \\
0 & 0 & 0 & 0 & 0 & z_{18\,6} & 0 & 0 & 0 & 0 & 0 & z_{18\,12} & 0 & 0 & 0 & 0 & 0 & z_{18\,18}
\end{bmatrix}
\begin{bmatrix}
\dot{L_1}^1 \\ \dot{P_e}^1 \\ \dot{h_{out}}^1 \\ \dot{T}_{wall,1}{}^1 \\ \dot{T}_{wall,2}{}^1 \\ \dot{m}_{out}{}^1 \\ \dot{L_1}^2 \\ \dot{P_e}^2 \\ \dot{h_{out}}^2 \\ \dot{T}_{wall,1}{}^2 \\ \dot{T}_{wall,2}{}^2 \\ \dot{m}_{out}{}^2 \\ \dot{L_1}^3 \\ \dot{P_e}^3 \\ \dot{h_{out}}^3 \\ \dot{T}_{wall,1}{}^3 \\ \dot{T}_{wall,2}{}^3 \\ \dot{m}_{out}{}^3
\end{bmatrix}
$$

$$
= \begin{bmatrix}
\dot{m}_{r,i}{}^1 h_{r,i}{}^1 + \alpha_{i1}{}^1 A_i{}^1 \left(\frac{L_1{}^1}{L_{total}{}^1}\right)\left(T_{w1}{}^1 - T_{r1}{}^1\right) \\
\alpha_{i2}{}^1 A_i{}^1 \left(\frac{L_2{}^1}{L_{total}{}^1}\right)\left(T_{w2}{}^1 - T_{r2}{}^1\right) \\
\dot{m}_{r,i}{}^1 \\
\alpha_{i1}{}^1 A_i{}^1 \left(T_{r,1}{}^1 - T_{w,1}{}^1\right) + \alpha_o{}^1 A_o{}^1 \left(T_a{}^1 - T_{w,1}{}^1\right) \\
\alpha_{i2}{}^1 A_i{}^1 \left(T_{r,2}{}^1 - T_{w,2}{}^1\right) + \alpha_o{}^1 A_o{}^1 \left(T_a{}^1 - T_{w,2}{}^1\right) \\
0 \\
\dot{m}_{r,i}{}^2 h_{r,i}{}^2 + \alpha_{i1}{}^2 A_i{}^2 \left(\frac{L_1{}^2}{L_{total}{}^2}\right)\left(T_{w1}{}^2 - T_{r1}{}^2\right) \\
\alpha_{i2}{}^2 A_i{}^2 \left(\frac{L_2{}^2}{L_{total}{}^2}\right)\left(T_{w2}{}^2 - T_{r2}{}^2\right) \\
\dot{m}_{r,i}{}^2 \\
\alpha_{i1}{}^2 A_i{}^2 \left(T_{r,1}{}^2 - T_{w,1}{}^2\right) + \alpha_o{}^2 A_o{}^2 \left(T_a{}^2 - T_{w,1}{}^2\right) \\
\alpha_{i2}{}^2 A_i{}^2 \left(T_{r,2}{}^2 - T_{w,2}{}^2\right) + \alpha_o{}^2 A_o{}^2 \left(T_a{}^2 - T_{w,2}{}^2\right) \\
\dot{m}_{r,i}{}^3 h_{r,i}{}^3 + \alpha_{i1}{}^3 A_i{}^3 \left(\frac{L_1{}^3}{L_{total}{}^3}\right)\left(T_{w1}{}^3 - T_{r1}{}^3\right) \\
\alpha_{i2}{}^3 A_i{}^3 \left(\frac{L_2{}^3}{L_{total}{}^3}\right)\left(T_{w2}{}^3 - T_{r2}{}^3\right) \\
\dot{m}_{r,i}{}^3 \\
\alpha_{i1}{}^3 A_i{}^3 \left(T_{r,1}{}^3 - T_{w,1}{}^3\right) + \alpha_o{}^3 A_o{}^3 \left(T_a{}^3 - T_{w,1}{}^3\right) \\
\alpha_{i2}{}^3 A_i{}^3 \left(T_{r,2}{}^3 - T_{w,2}{}^3\right) + \alpha_o{}^3 A_o{}^3 \left(T_a{}^3 - T_{w,2}{}^3\right) \\
0 \\
\dot{m}_{comp.}
\end{bmatrix} \tag{8}
$$

The algebraic differential equations in the form of equation 8 were converted into an executable format in the MATLAB/SIMULINK framework and solved at discrete time steps.

3.2.1 Evaporator Fan Map

A team of senior students performed tests to develop a map for the evaporator fans. The voltage across the fans was changed discreetly using the DAQ system and the corresponding fan power and air velocity was measured. The power consumed by fans is measured by using the laboratory Mulitmeter and the mass flow rate of the air is calculated by the equation 9.

$$\dot{m}_{air} = \rho_{air} A v \tag{9}$$

Where, A is the measured area of the cross-section of air flow, v is the velocity of air measured by an anemometer and ρ_{air} is the density of the air at room temperature.

Figure 3-2 and Figure 3-3 gives the curves for the corresponding measured data points for the fan power and the air flow rate.

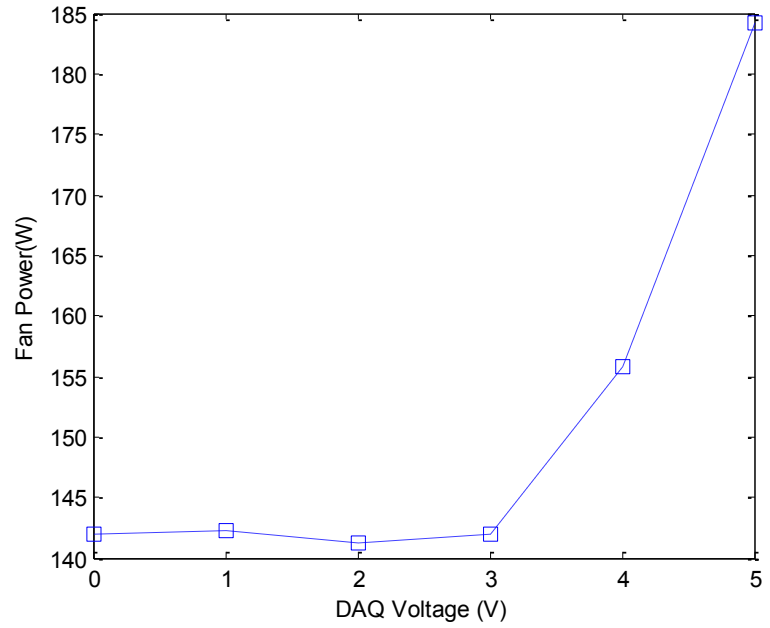

Figure 3-2 DAQ Voltage vs. Fan Power

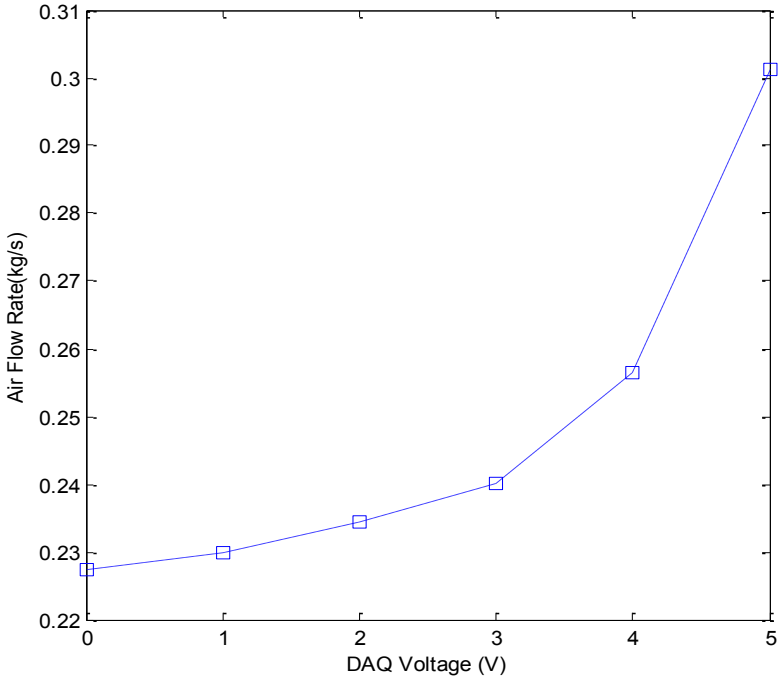

Figure 3-3 DAQ Voltage vs. Air Flow Rate

3.3 Compressor Modeling

The compressor used in this study is a positive displacement, reciprocating type gas compressor. Its modeling is done based on the static relationships. This approach is characterized by determining the mass flow rate of the refrigerant and the outlet fluid enthalpy at the compressor exit. Equations 10 and 11 give the algebraic formulas used to determine the mass flow rate and enthalpy at the enthalpy at the compressor outlet.

$$\dot{m}_k = \omega_k V_k \rho_k \eta_{vol} \tag{10}$$

$$h_{out} = \frac{1}{\eta_k}[h_{out,isentropic} + h_{in}(\eta_k - 1)] \tag{11}$$

Here $\dot{m}_k$ is the mass flow rate of the compressor, ω_k is the speed of the compressor in rpm, V_k is the volume of the compressor, ρ_k is the density of the refrigerant at the compressor inlet, h_{in}, h_{out} and $h_{out,isentropic}$ are the enthalpies of the refrigerant at the inlet, outlet and the outlet enthalpy if it goes through an isentropic process in the compressor. η_{vol}, η_k are the volumetric and adiabatic efficiencies of the compressor which are generally modeled using an empirical relationship based on the pressure ratio and the speed of the compressor, $\eta_{vol} = f_1(P_{ratio}, \omega_k)$ and $\eta_k = f_2(P_{ratio}, \omega_k)$. However, in this study the compressor used is a constant speed drive, so the semi-empirical map was not created and typical values of volumetric and isentropic are estimated as, $\eta_{vol} = 80\%$ and $\eta_k = 90\%$. The estimation is done by running the system and taking the ratio of the theoretical compressor mass flow rate as given in equation 10 and the experimentally measured refrigerant mass flow rate to obtain the

mass flow rate correction factor. This correction factor when multiplied with an initial guess value of the volumetric efficiency provides the estimated value.

3.4 Expansion Valve Modeling

The expansion valves are the primary means for metering the mass flow of the refrigerant in a vapor compression system. The expansion valves used in this research are the MEMS based Silicon Expansion Valves (SEVs) whose characteristics are discussed earlier in Section 1 of this thesis. Their modeling is done using the orifice as shown in equation 12,

$$\dot{m}_v = C_d A_v \sqrt{\rho(P_c - P_e)} \tag{12}$$

Where C_d is the coefficient of discharge, $\dot{m}_v$ is the mass flow rate of the valve, A_v is the area of the valve opening, P_c is the condenser pressure, P_e is the evaporator pressure and ρ is the refrigerant density at the valve inlet.

The expansion process through the valve is assumed to be isenthalpic; therefore the inlet and the exit refrigerant enthalpy are the same as given in equation 13.

$$h_{v,in} = h_{v,out} \tag{13}$$

The coefficient of discharge C_d is an empirical entity which depends on the geometry of the valve and the fluid properties. Also, the valve area A_v cannot be directly determined. The product of the coefficient of discharge and area of valve opening is calculated from semi-empirical maps as a function of the pressure differential across the valve, $\Delta P = P_{in} - P_{out}$, and the valve opening input, u_v as shown in Equation 14.

$$A_v C_d = f(u_v, \Delta P) \tag{14}$$

3.4.1 Expansion Valve Map

The empirical map for the valve was created by running the system at different valve openings. The corresponding pressure differential across the valve and mass flow rates were recorded and equation 11 was used to fit a curve for the product of the coefficient of discharge and the valve area as $K = A_v C_d$ vs. the pressure differential and the valve opening. Figure 3-4 shows the SEV data points and the corresponding curve fit for those points.

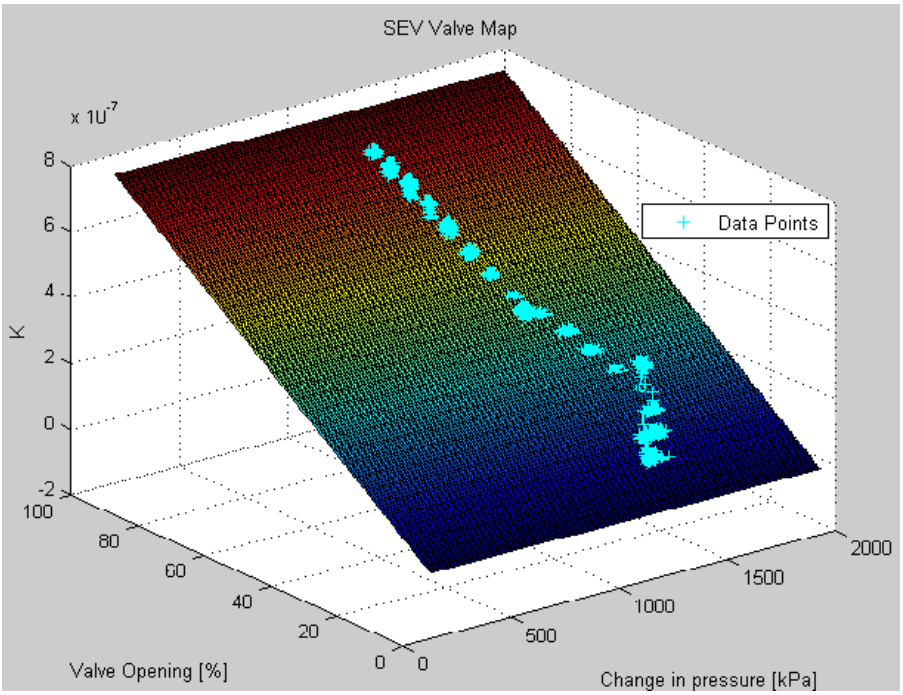

Figure 3-4 Curve Fit for SEV Map

4. MODEL VALIDATION AND SIMULATION RESULTS

The experimental system as described in Section 2 of this thesis was used to run tests and validate the simulation models with the experimental data. This section will deal primarily with the methodology used in translating the mathematical models derived in before into executable models in the MATLAB/SIMULINK. The file structures used to simulate component models along with structures used to reference parameters such as thermal parametric variables, operating conditions and physical parameters of component models are also be addressed. Later in this section the simulation results are presented.

4.1 Model Startup

Transient simulation is generally performed by starting the system at a known equilibrium condition, and observing the system response to changes in the external inputs. Thus given a set of parameters and steady-state inputs, $u(0)$ the values of the state variables are found, $x(0)$ using Equation 15.

$$0 = f(x(0), u(0)) \tag{15}$$

The equilibrium conditions are largely defined by ensuring steady-state energy balances. Thus initializing the dynamic models requires data obtained at steady-state conditions so that unknown empirical parameters may be determined, e.g. heat transfer coefficients. To start the models, an initialization file is loaded in the MATLAB workspace which details all the system parameters and the support files.

4.1.1 Parametric Variable Structure

The dynamic models are initialized by first loading the Physical Parameters structure and then the Operating Parameter structure in MATLAB workspace. These variables are accessed as global variables from the MATLAB® workspace by the models during simulation. The fluid property variable, 'RefProp' refers to properties of the current refrigerant being used in the simulation i.e. R404a. Similarly the variables 'Air' refer to parameters needed for the simulations for the evaporator side secondary fluid. Table 4-1 below gives the parametric variable structure used in the modeling.

Table 4-1 Parametric Variable Structure

Structure name	Description
RefProp	refrigerant properties R404a
Air	air properties
Physical_Parameters	physical characteristics of components
Operating_Conditions	measurable quantities defining the base operating point

The Physical_Parameters variable structure is a user defined list of parameters which describe the physical characteristics of the component model. The Operating_Conditions structure describe in terms of measurable quantities like pressures, temperatures, mass flow rates which define the base operating point at which the model is simulated. In this thesis, the operating conditions used for initialization are always the steady state values obtained from the experimental system. Table 4-2 gives

the complete list of physical parameters of a single evaporator, the expansion valve and the compressor.

Table 4-2 Physical Parameter Structure of the Components

Component	Parameter	Units	Formula used	Value	Comment
Evaporator	Number of Fins	-	-	120	Counted
	Fin Spacing	$[m]$	-	0.0084	Calculated
	Total Mass (including fins)	$[kg]$	$\rho\pi(R-r)^2 l$ + Mass of Fins	6.486	Calculated
	Specific Heat	$[kJkg^{-1}K^{-1}]$	-	0.9	Aluminum
	Surface Area (external)	$[m^2]$	πDl + Fin Area	19.541	Tuned
	Surface Area (internal)	$[m^2]$	πdl	1.8637	Tuned
	Cross-sectional Area	$[m^2]$	$\pi d^2/4$	5.8e-5	Calculated
	Length (l)	$[m]$	-	34.49	Measured
	Outer Diameter(D)	$[m]$	-	0.0095	Measured
	Inner Diameter (d)	$[m]$	-	0.0086	Estimated
	Slip Ratio	-	-	4	Tuned
Expansion Valve	Valve Opening Upper Limit	[%]	–	100	Manufacturer Data Sheet
	Valve Opening Lower Limit	[%]	-	0	Manufacturer Data Sheet
	Rising Slew Rate	$[s^{-1}]$	–	100	Estimated
	Falling Slew Rate	$[s^{-1}]$	–	-100	Estimated
	Delay	$[s]$	-	0	Estimated
Compressor	Displacement	$[m^3]$	-	8e-5	Manufacture Data Sheet
	Speed	$[rpm]$	-	1750	Manufacture Data Sheet

4.1.2 Refrigerant Properties

A refrigerant property generation R404A_v1.mat file is used for adding fluid properties into the model. The fluid property calculations during simulation are implemented using 1-D or 2-D look table blocks provided in Simulink and customized blocks for all the calculated thermal properties. The lookup tables are separated into three sections: saturated properties, liquid properties, and vapor properties. The thermal properties of the refrigerant are determined by interpolating or extrapolating these set of values for a given state of refrigerant defined by its temperature, pressure or the enthalpy.

4.1.3 Steady State Solvers

The steady state solver files are used as the constraint functions such as the *fmincon* function provided in MATLAB. It is used to calculate the optimal initial condition solution based on the given operating conditions and physical parameters. It outputs the initial values for the state vector.

4.1.4 Heat Transfer Coefficient Correlations

The model requires a collection of correlation sub routines for the calculation of heat transfer coefficients for both the two phase and single phase refrigerant flows and for heat transfer coefficient between the heat exchanger wall and the external fluid. In the case of the evaporator the heat transfer coefficient for the two phase region is calculated using the Wattelet-Chato correlation [28] and the single phase refrigerant flow heat transfer coefficient is calculated using the Gnielinski correlation [29]. The initial guess for the heat transfer coefficient for the heat exchanger wall and the external fluid is

obtained by first doing a steady state energy balance between the air side and the refrigerant side heat transfer. Given the refrigerant side heat transfer coefficients, twelve simultaneous equations are then solved to get the initial values for air side heat transfer coefficients, two-phase flow length, and the wall temperatures for two phase and the superheated region for the three evaporators.

4.2 Simulation Results

The dynamic models were started at the steady state and the response of the system for step changes to the valve opening was observed. Three cases of external step changes were studied.

Case 1: Valve for evaporator one was closed from 60% to 30% while the valves for evaporator 2 and evaporator 3 were kept at constant opening of 50% as shown in Figure 4-1. Figure 4-2 - Figure 4-5 compares the response of the system and the experimental data.

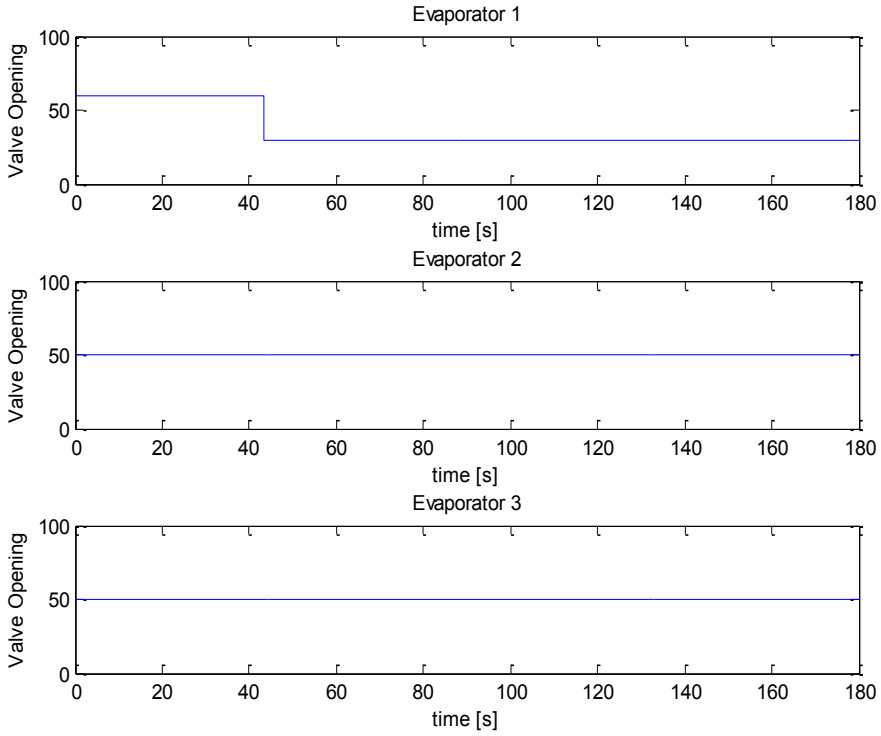

Figure 4-1 Step Input to the Expansion Valve 1

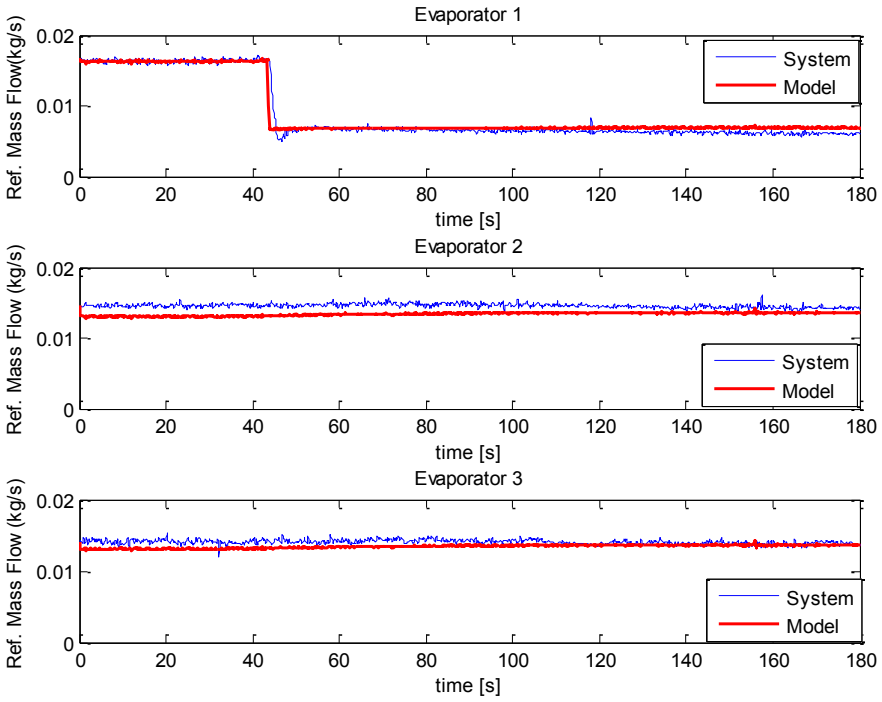

Figure 4-2 Refrigerant Mass Flow Rate at the Evaporator Inlet for Case 1

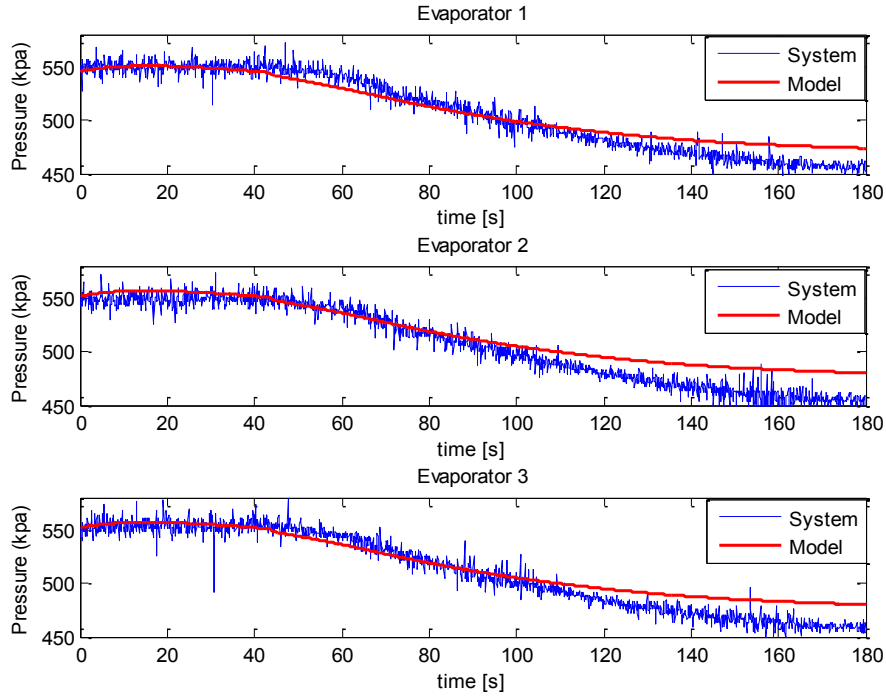

Figure 4-3 Refrigerant Pressure at the Evaporator for Case 1

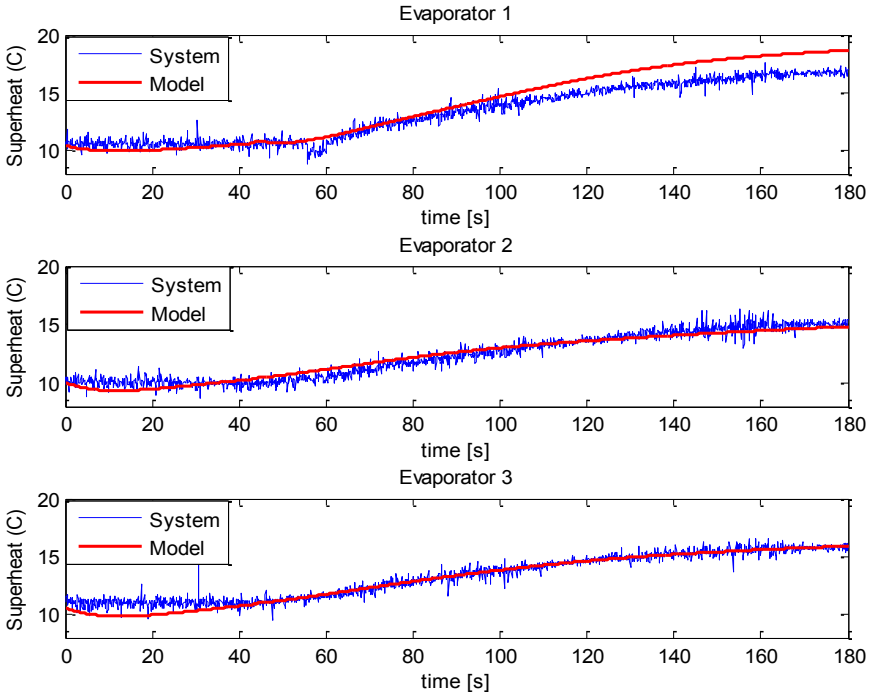

Figure 4-4 Refrigerant Superheat at the Evaporator Outlet for Case 1

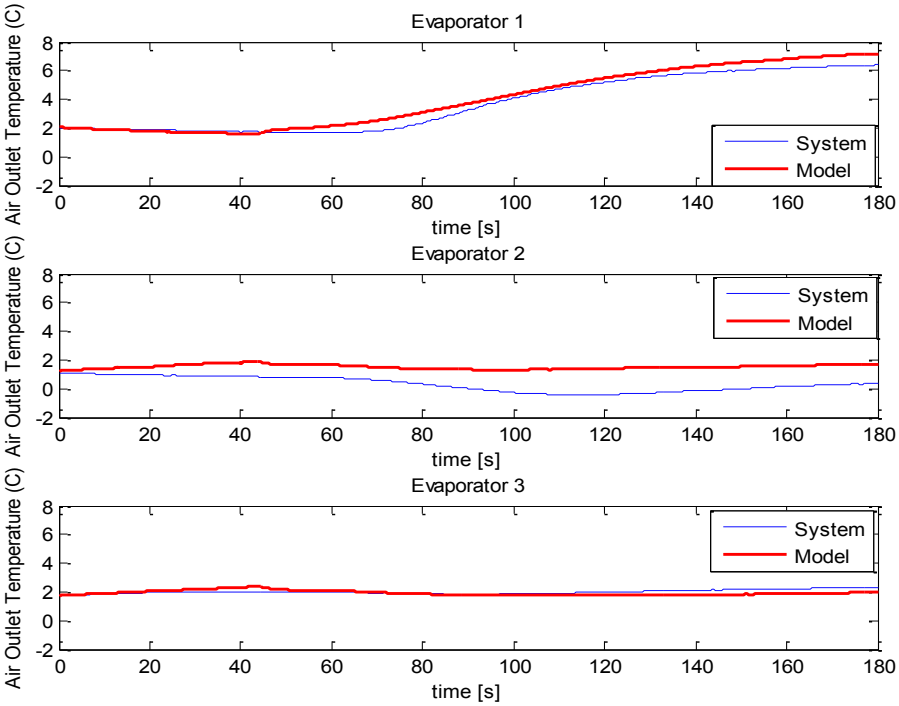

Figure 4-5 Air Temperature at the Evaporator Outlet for Case 1

Case 2: The system was started with all the valves opened at 60%. Valve for evaporator two was first closed from 60% to 30% and the valve for evaporator 3 was later opened to 80%. Valve for evaporator 1 was kept at constant opening of 60% as shown in Figure 4-6. Figure 4-7 - Figure 4-10 compares the response of the system and the experimental data.

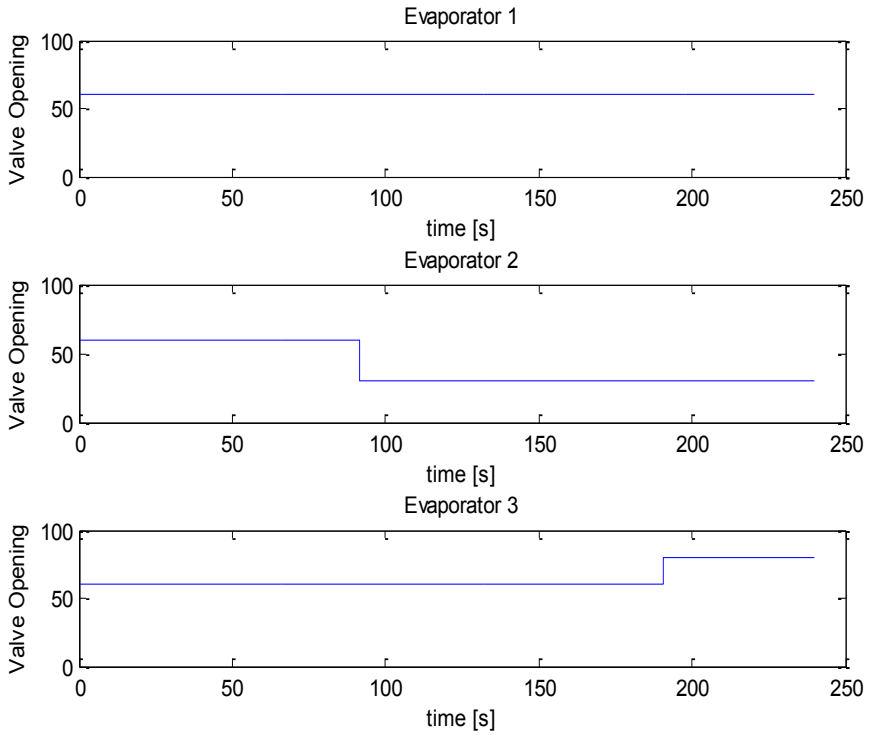

Figure 4-6 Step Input to the Expansion Valve 2 and Valve 3

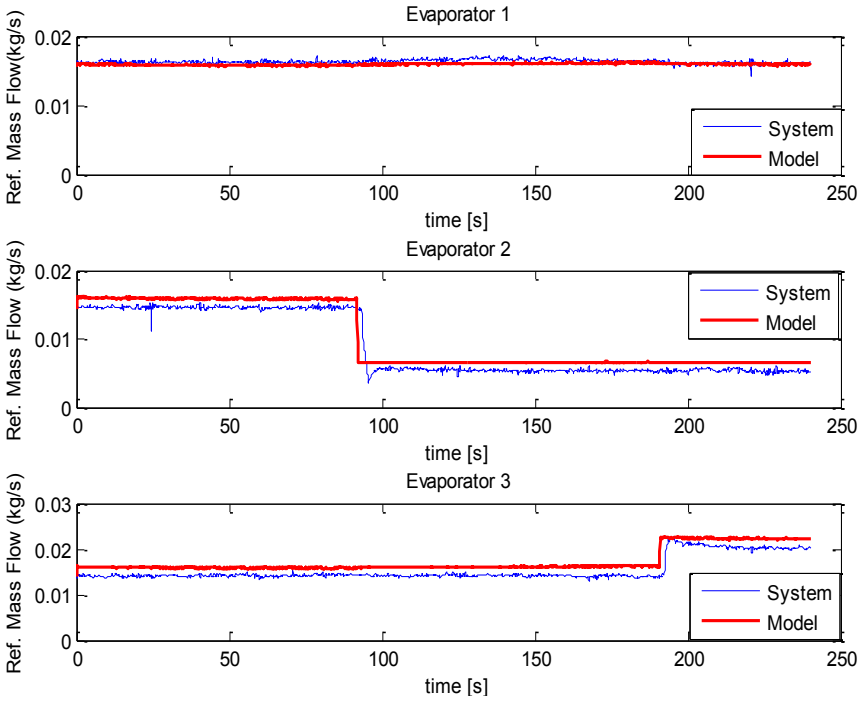

Figure 4-7 Refrigerant Mass Flow Rate at the Evaporator Inlet for Case 2

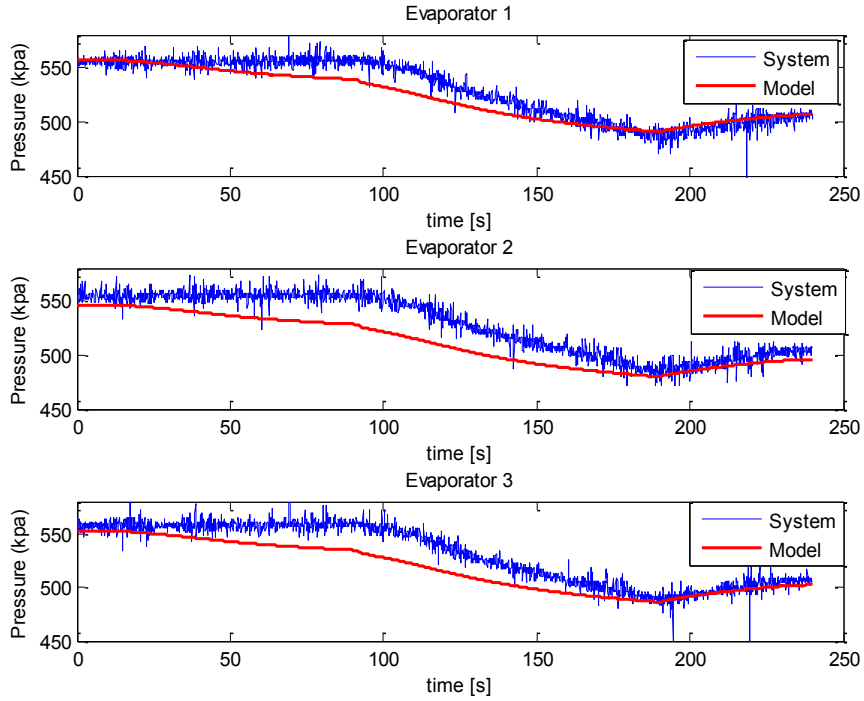

Figure 4-8 Refrigerant Pressure at the Evaporator for Case 2

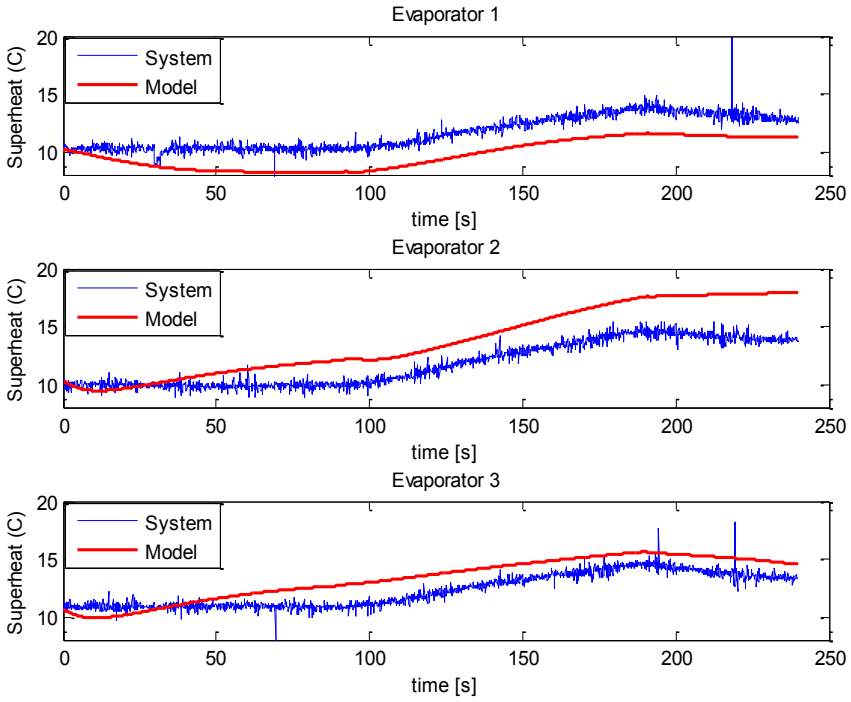

Figure 4-9 Refrigerant Superheat at the Evaporator for Case 2

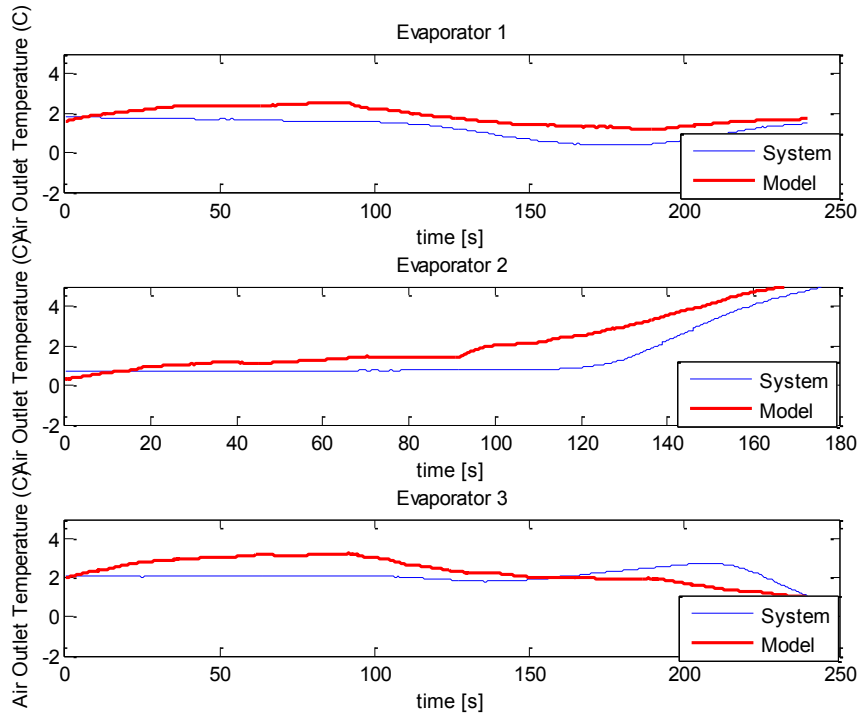

Figure 4-10 Air Temperature at the Evaporator Outlet for Case 2

Case 3: The system was started with all the valves opened at 60%. Each valve was closed from 70% to 50% at different time intervals as shown in Figure 4-11. Figure 4-12- Figure 4-15 compares the response of the system and the experimental data.

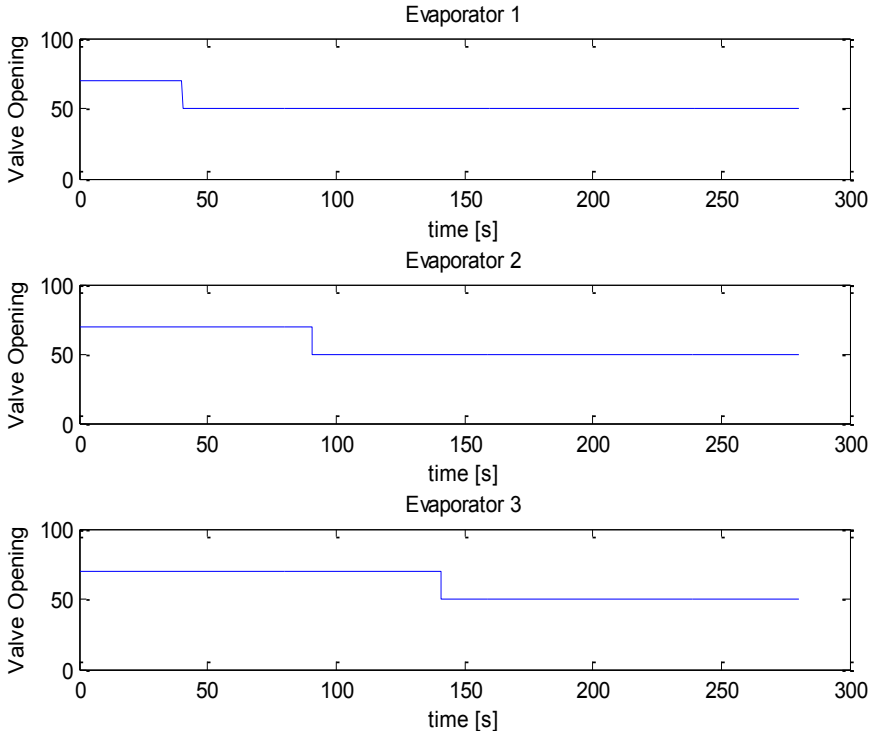

Figure 4-11 Step Input to Expansion Valves

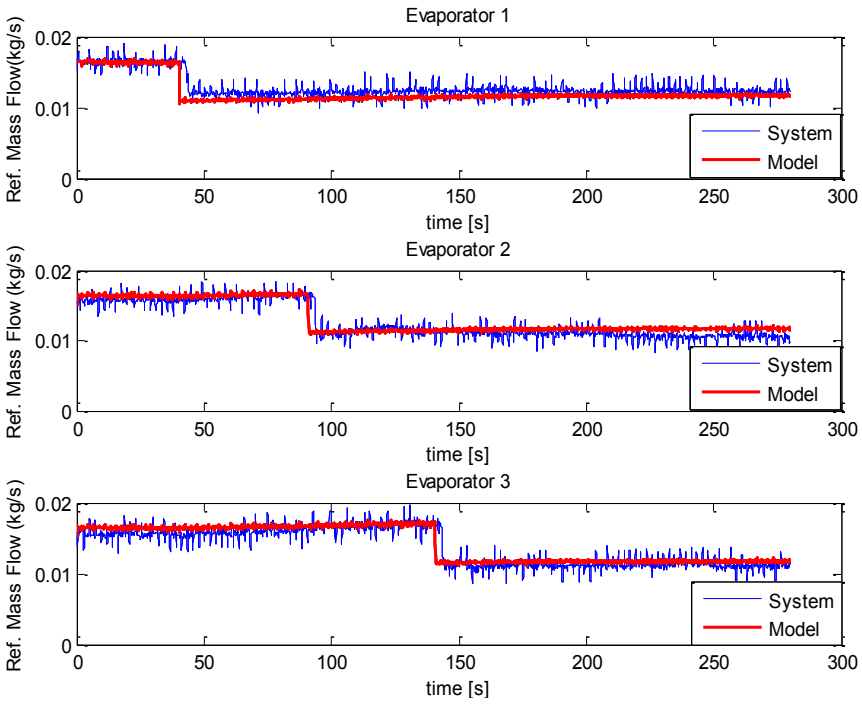

Figure 4-12 Refrigerant Mass Flow Rate at Evaporator Inlet for Case 3

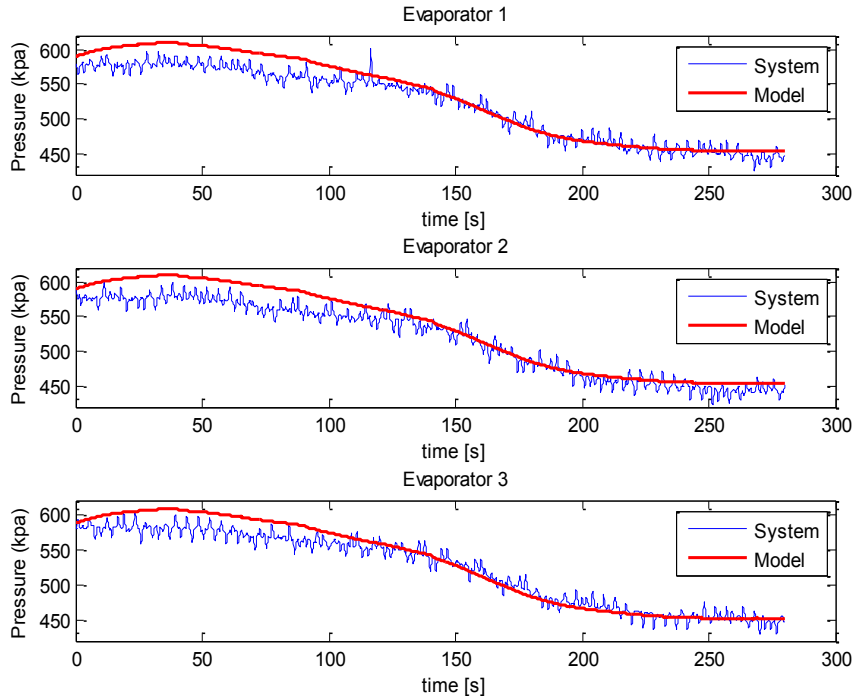

Figure 4-13 Refrigerant Pressure at the Evaporator for Case 3

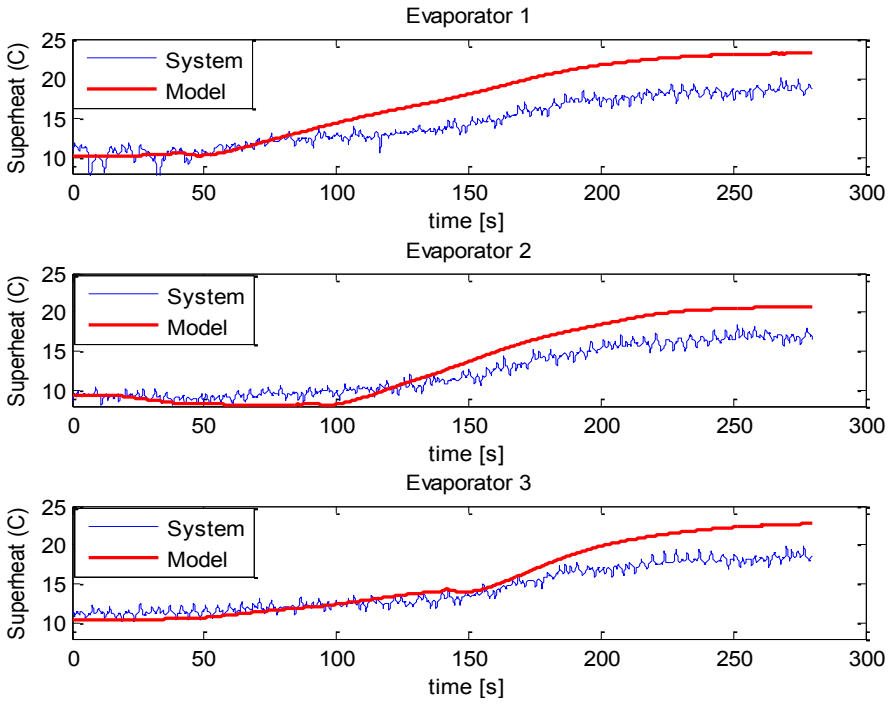

Figure 4-14 Refrigerant Superheat at the Evaporator Outlet for Case 3

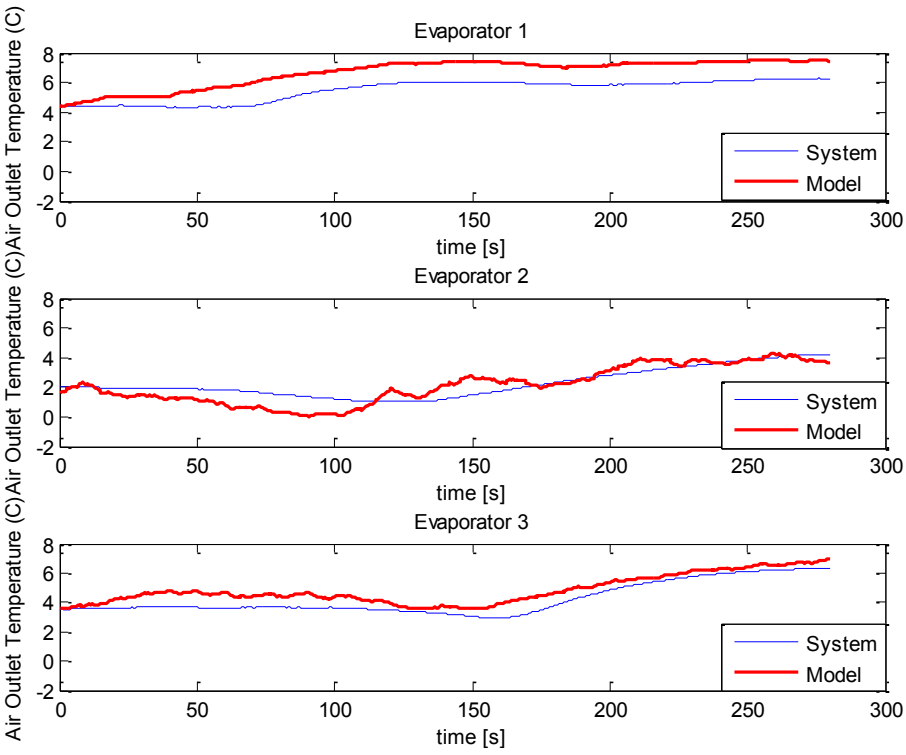

Figure 4-15 Air Temperature at the Evaporator Outlet for Case 3

4.2.1 Observations

The simulation results for the three cases discussed above indicate that the models are capable of fairly capturing the dynamics of the multi-evaporator system. The transient responses for the pressures seem to match well with some offset at the steady state for case 1. Similarly in case 2 there is slight mismatch in the initial steady state variation of the pressure and the superheat. The outlet temperatures predicted by the models and the experiments also differ by some amount. One reason for this discrepancy may be that there in only one thermocouple which measures the temperature of air at the evaporator outlet for its entire length (41 inches). This discrepancy can be reduced if more thermocouples are installed and spread over the length of each evaporator. The average values can be recorded which should provide more accuracy in the experimental and modeling results. But the overall system response and the simulation results look satisfactory.

The output transient response of the models is impervious to slight changes in the physical changes. However, the models are highly sensitive to changes in the values of the external air heat transfer coefficients. The way models calculate the external heat transfer coefficient values is explained in sub-section 4.1.4. Different values for the two-phase heat transfer coefficients also affect the transient response drastically as it can change the initial length of the two phase flow which has a considerable impact on the output response. The transient response of the system shows that the models are also very sensitive to the refrigerant mass flow rate changes.

5. CASCADED CONTROLLER DESIGN FOR SUPERMARKET REFRIGERATION SYSTEM

For years, evaporator superheat control is a perennial problem in the HVAC&R industry. This can be achieved by using the traditional Thermostatic Expansion Valves (TEVs), or the Electronic Expansion Valves (EEVs) based on simple PID loops or most recently the cascaded control algorithm for the MEMS based Silicon Expansion Valves (SEVs). This section gives the background of the cascaded controller, followed by its advantages and finally the experimental results for the design of cascaded control architecture on the supermarket refrigeration. The experimental results compare the performance of the TEVs, the Microstaq Superheat Controller (SHC) and the SEVs with cascaded controller.

5.1 Cascaded Controller Background

As a general practice in industries, the control of superheat in a multi-evaporator system is achieved by the TEVs or the Automatic Expansion Valves (AEVs). These standard mechanical devices can operate effectively under the design conditions but show degraded performance under transient operation such as valve hunting in case of TEVs. With technology advancement, the EEVs allow more sophisticated approaches where an external signal from a computer based algorithm is used to regulate the valve opening, resulting in superior superheat control. The use of EEVs has overcome the problem of valve hunting. But researchers have found that poorly tuned EEVs result in

undesirable system behavior and frequent tuning of the control gains are required. The need to regularly schedule controller gains also raises concerns about the valve longevity. Rasmussen et al. [30] proposed the use of Hybrid Expansion Valves (HEVs) which combine the mechanical and electronic actuation and provide enhanced superheat regulation. In an Automatic Expansion Valve (AEV) a spring is used to mechanically apply force on the diaphragm to regulate evaporator pressure. While in EEVs a stepper motor is given an external signal which in turn opens or closes the valve. A Hybrid Expansion Valve can be viewed as a device which augments a standard AEV and an EEV. In a HEV the stepper motor is used to provide linear force in the spring which in turn exerts pressure on the flexible diaphragm. This results in significant reduction in electronic actuation and also increases the valve life. A complete description about the design and working of a HEV can be found in their publication [30]. Their paper discusses the working of the TEVs, AEVs, EEVs and the HEVs and compares the system characteristics based on different superheat control mechanisms. Their experimental setup was a 3 ton residential air conditioning system which was used to compare the control performance of HEV vs. TEV and AEV and a 0.5 ton water chiller system which was used to compare HEV vs. EEV. The systems were subjected to internal (compressor speed step changes), external (secondary fluid flow rate changes) and periodic transient disturbances. Their results indicate that the control effort was least with the HEVs. The metering control strategy was superior for HEVs in both the steady state and the transient operating range of the system.

Most recent research has led to the development of MEMS based valve technology. These valves are of very small size and weight and have no mechanical parts which make them impervious to fatigue failure. Due to commercial confidentiality there are only fewer publication examining the functioning and performance of MEMS valves. Jeff Uibel compared the performance of a 3 silicon-plate MEMS valve and a solenoid valve for an automotive air-conditioner [31]. He showed that the performance of the MEMS valve was comparable to the solenoid valves in terms of controlling the fluid pressure in excess of 2000 psi and the flow rates were comparable to the solenoid valves. Rasmussen and Elliott [32] have emulated the control mechanism of the HEV on the Electronic Expansion Valve and the MEMS based Silicon Expansion Valve (SEV). To emulate the behavior of a HEV two control loops can be combined: a fast pressure control loop with mechanical feedback and a slow superheat control loop that changes the evaporator pressure in order to keep superheat constant. This gives rise to the Cascaded Control Loop. A schematic of the algorithm is given in Figure 5-1.

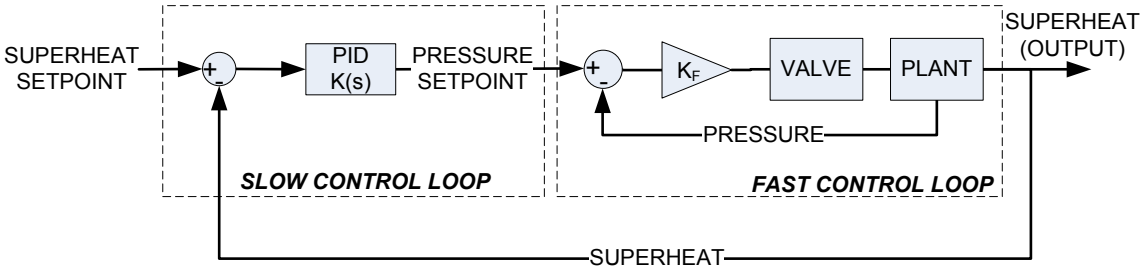

Figure 5-1 Cascaded Control Loop

In their paper [32], they compared the performance of HEV vs. SEV with HEV emulation using cascaded control vs. EEV with standard PID controller based on superheat reference point tracking and external disturbance rejection when the compressor speed changes abruptly. Their results indicate that SEVs provide superior superheat control by emulation of the HEVs using the cascaded control loop than the EEVs with simple PID loop. Furthermore, when the same HEV emulation was carried out on an EEV it failed to respond fast enough to internal transient disturbances due to its physical hardware limitations. It was concluded that for a successful HEV emulation the SEV is better suited than an EEV, given it responds as quickly as the mechanical diaphragm of a HEV for pressure regulation along with continuous electronic actuation.

5.2 Advantages of Cascaded Control Architecture

There are lots of advantages of using a cascaded control algorithm which are subsequently discussed in this sub-section.

5.2.1 Non-Linearity Compensation

One of the advantages of using a cascaded control loop is that it compensates with the non-linearity of the system. Larsen et al [33] proposed a control architecture in which an inner loop regulated the refrigerant mass flow to a setpoint generated by an outer linear PID loop. Although their approach significantly linearized the evaporator response to the controller but it requires an additional sensor to measure the refrigerant mass flow. Elliott and Rasmussen overcame the issue of additional mass sensor by their cascaded control methodology discussed above, which only needs evaporator pressure

and refrigerant temperature at the evaporator outlet. In their publication [34] they implemented cascaded controller on a regular EEV and compared the results with a HEV. In general mass flow rate through an EEV is a non-linear function of the valve opening. This increases complexity in designing efficient PID or robust controllers for an EEV. They observed the superheat response to step changes in valve openings for high and low flows and found that both EEVs with cascaded controller and HEVs contributed to a significant non-linearity compensation of the system. The HEV lead to more non-linearity compensation due to the fact that HEV regulated pressure using mechanical spring and diaphragm which have high stiffness and hence higher internal gains. But in case of an EEV higher proportional gains to compensate for non-linearity cannot be implemented due to the inherent hardware limitations of the EEV. An actuator with higher bandwidth like the MEMS based SEVs will allow use of high proportional gain values in the cascaded loop due to their instantaneous response. Henceforth, they will serve as better HEV emulators and thus greater non-linearity compensation in the system.

5.2.2 Decoupling in Multi-Evaporator System Dynamics

Another benefit of using a cascaded algorithm is that it can be effectively used to control multi-evaporator systems. In a multi-evaporator system, the dynamics of each evaporator is tightly coupled with each other which decrease the efficacy of a decentralized controller. This leads to the use of complex Multiple-input, Multiple-output (MIMO) control techniques for such systems. It has been found that using a cascaded control methodology on a MIMO system helps in decoupling the system

dynamics. Elliott and Rasmussen carried experimental investigation on a two-evaporator water chiller system based on SEVs with cascaded architecture and traditional PID controllers. Firstly, they carried Relative Gain Array (RGA) analysis which gives a parameter to measure coupling between Single-input, Single-output (SISO) pairs. The closer the RGA number is to zero, the more decoupled is the system dynamics [35]. In their paper [36] it was found that for a particular value of inner proportional gain of the cascaded control the RGA number becomes zero indicating decoupled dynamics between the two evaporators. They further carried superheat reference tracking, disturbance rejection and pull down tests at compressor start-up which resulted in decoupling by the cascaded controller compared to the traditional PIDs. The separation of evaporator dynamics observed by the cascaded control also implies that stable superheats can be achieved quickly.

5.3 Implementation of Cascaded Control on Supermarket Refrigeration System

The cascaded control architecture has proved to provide superior superheat regulation results for the multi-evaporator system based on the Silicon Expansion Valves as discussed above. The same control methodology was implemented to regulate the superheat for individual evaporators of the supermarket refrigeration system. The SEVs accept a 0% to 100% valve opening signal from the DAQ PC which is converted to a 0-5 V pulse width modulation (PWM) voltage signal which in turn controls the valve opening. The response time is observed to be in milliseconds. Figure 5-2 gives the design of controller for the three evaporator supermarket refrigeration system.

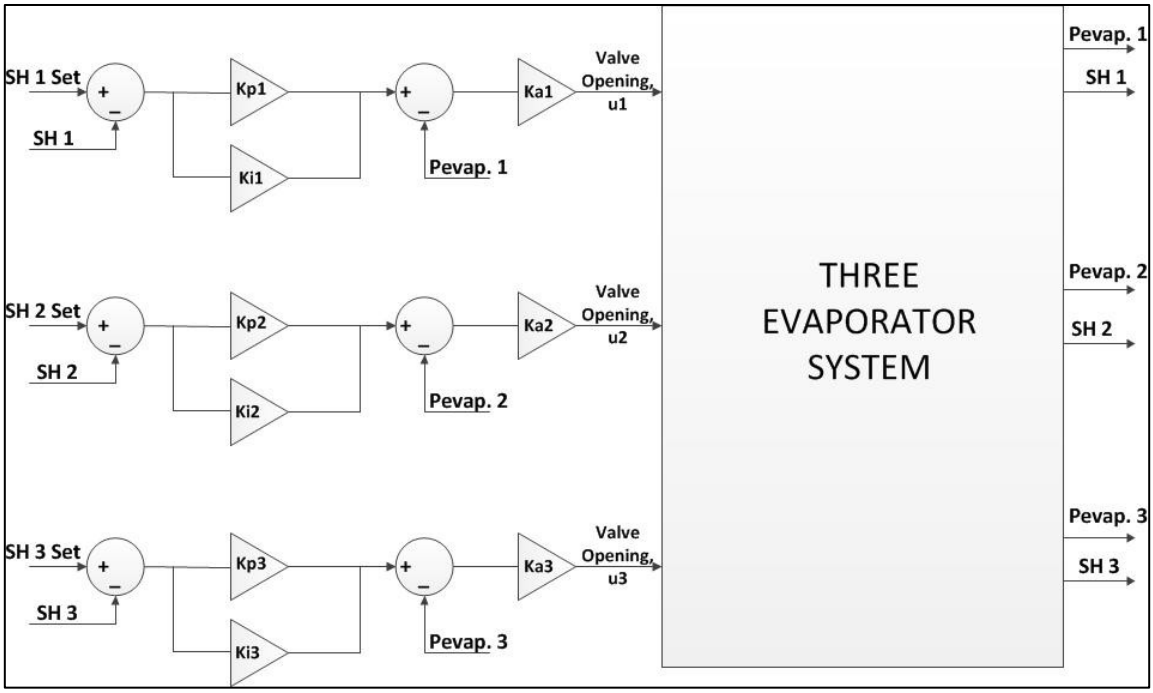

Figure 5-2 Cascaded Controller for the Three Evaporator System

The next subsection gives the experimental results obtained after the design of the controller.

5.3.1 Experimental Results

A comparative study was done to analyze the system cooling and superheat control with the TEVs, SEVs with Microstaq Superheat Controller, and SEVs with our designed controller. The objective of this study is to analyze efficiency gains when a cascaded controller or the commercial controller based on SEVs are used in place of the standard mechanical valves. The efficiency gains in this study are analyzed in terms of 1) Superheat Regulation. 2) Cooling and Power Consumed by the system. 3) COP of the system. Usually in supermarkets, the display cases run for 24 hours a day with periodic compressor on-off cycles with a couple or more defrost cycles in day. The compressor

on-off is automatically triggered by the discharge air temperature thermostat installed in such supermarket refrigeration display cases. In our experimental system, the unit is designed to shut off by itself when the discharge air temperature scales down to -1.1 ˚C (30 ˚F).

Superheat Regulation

Superheat regulation is a perennial problem in the HVAC industry. In this test case, the system was run on the TEVs first, followed by the SEVs using the MS Superheat Controller and finally the SEVs with the cascaded controller. The cascaded controller was also made to shut off the valves completely at the compressor shut down. The idea behind it is to reduce the amount of cooling lost when the compressor shuts off and then starts up again. Figure 5-3 shows a comparative response of three evaporators' superheat. The comparison for the TEVs, the commercial controller and the cascaded controller is done for two compressor on-off cycles. The reference set point for the superheat is 8 ˚C.

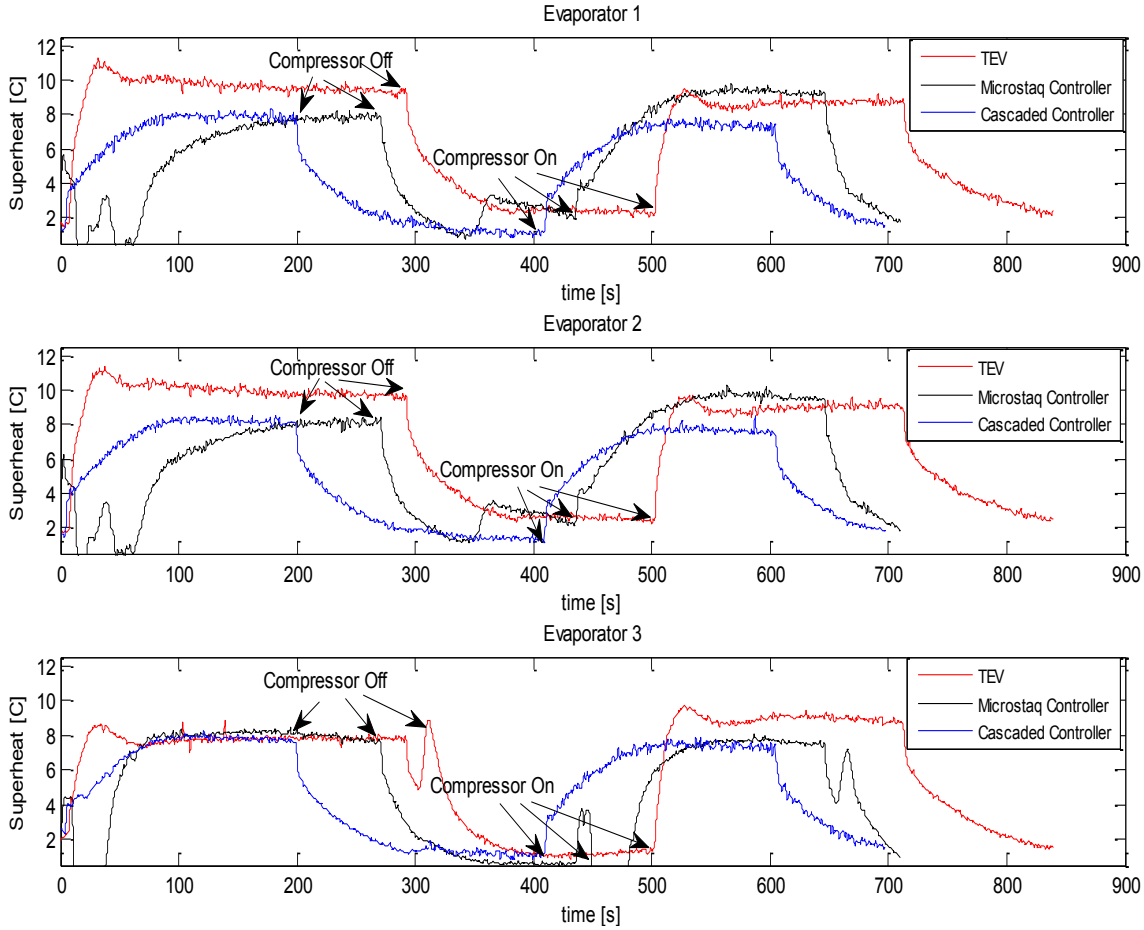

Figure 5-3 Superheat Response for the Three Evaporators

As shown in the plot above, after the compressor startup at t=0 seconds, the TEVs settled down at a higher superheat of about 9.5 ˚C. The commercial superheat controller also showed some steady state error. The reference point of the superheat is best seen to be tracked by the cascaded controller. The reader should also notice that after the first compressor shut off the superheat goes down, but it is not completely zero, this is due to the fact that the evaporator fans were still on after the compressor shutdown which leads to the boiling of the refrigerant.

A comparison was made for the cascaded controller and the commercial controller for the refrigerant mass flow rate to the three evaporators as shown in Figure 5-4. The mass flow rate to the evaporators will correspond to the actuator behavior. Since, for the commercial superheat controllers the actual data logging for the valve opening and closing was not available so exact valve data could not be compared.

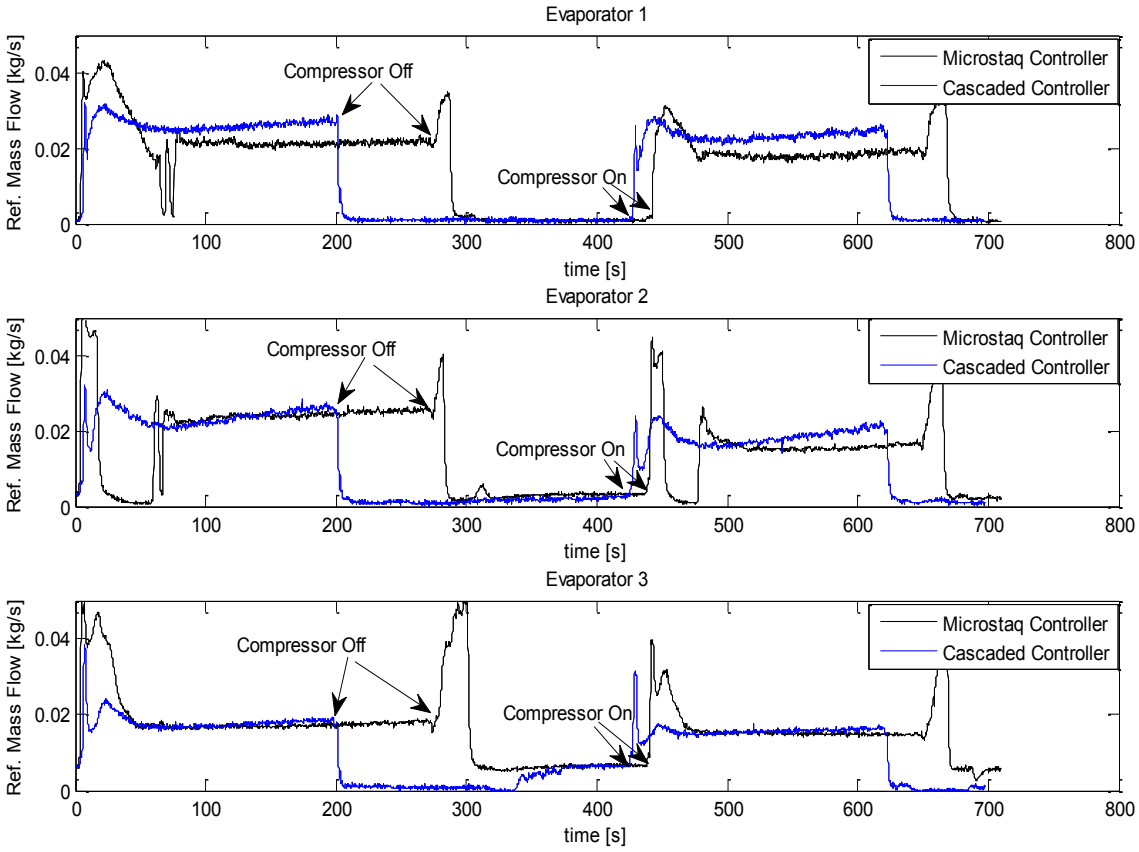

Figure 5-4 Refrigerant Mass Flow Rate to the Evaporators

From the plot above, the reader can notice that at the compressor shut-down there is a spike in the refrigerant mass flow rate for the commercial controller which corresponds to a sudden opening of the valves. While in the design of the cascaded

control, the valves were made to shut-off completely at the compressor shut-down which is reflected by the sudden decrease in refrigerant mass flow rate.

Cooling & Power Consumed by the System

Another comparison was made for the three control mechanisms in terms of overall cooling and the power consumed by the system. Figure 5-5 shows the total refrigerant side cooling of the system.

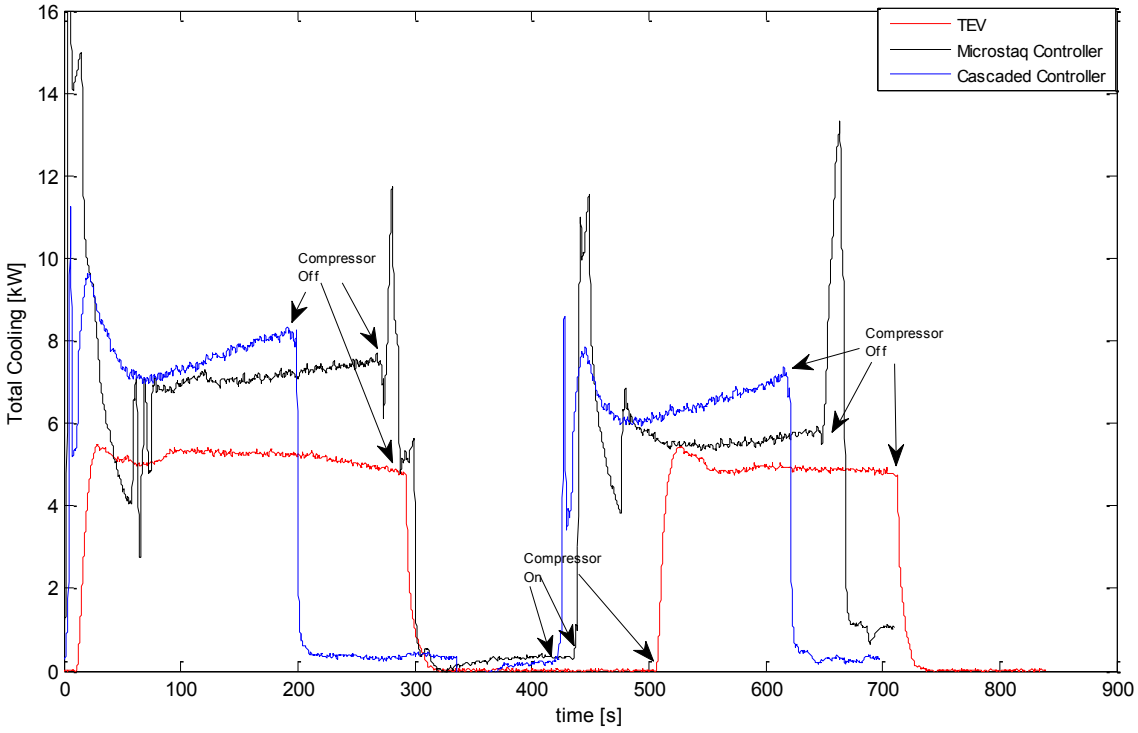

Figure 5-5 Total Refrigerant Side Cooling

As shown in the plot above, there is a significant improvement in the amount of refrigerant side cooling with the cascaded and the commercial controller, as compared to

the TEVs. It is also observed that the designed cascaded controller and the commercial controller forces the compressor to shut off earlier, reducing the total run-time of the compressor

If we look at the total power consumed by the system as shown in Figure 5-6, it will provide a clear picture about the compressor on-off cycle times. The system total power consumption includes the compressor, the evaporator fans and the lights which are measured by the Power Transducer.

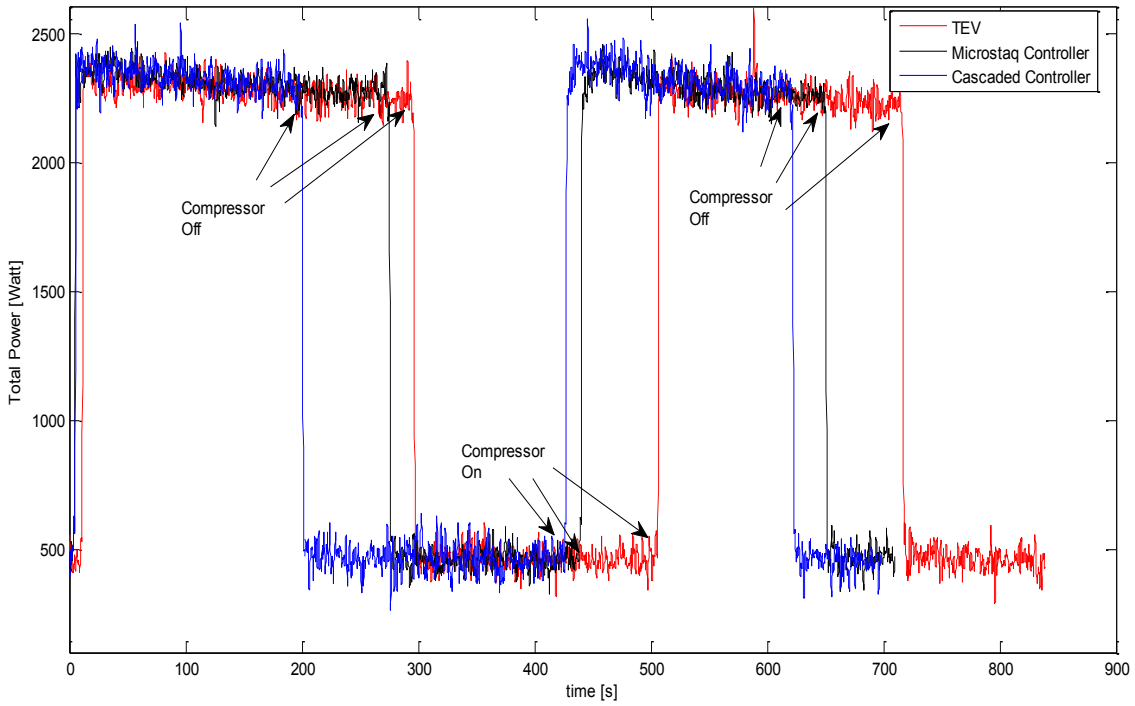

Figure 5-6 Total System Power (Compressor + Evaporator Fans + Lights)

The total run-time of the compressor was least for the cascaded controller, followed by the Microstaq controller and then the TEVs, for a time period of 700 s. The

superior cooling effects for both the cascaded and the MS controller force the compressor to shut down earlier as compared to the TEVs.

COP of the System

The Coefficient of Performance or the COP of the system is defined by equation 16.

$$COP = \frac{Total\ Cooling}{Total\ Power\ Consumed} \tag{16}$$

Figure 5-7 compares the COP of the system for the three actuators.

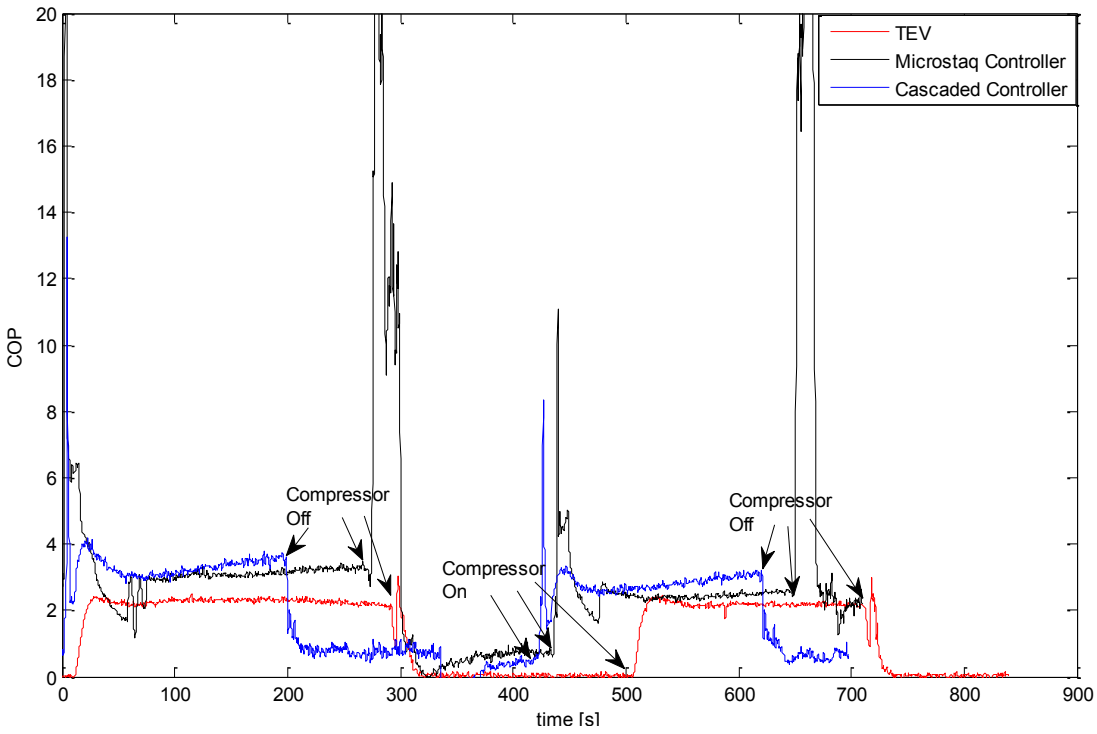

Figure 5-7 COP of the System

The COP comparison shows that both the MS and the cascaded controller performed much better than the mechanical valves and a slight gain in COP for the cascaded control over the Microstaq controller.

The system efficiency gains using the three actuators can be quantified by the performance indicators like cooling, power consumption, duty cycle and the COP of the system. The duty cycle in a square waveform is the ratio of the total high period to the total period. In our case, duty cycle will give the ratio of the total compressor runtime over the total time in one cycle. Table 5-1 gives the comparison of each individual control mechanism for their one compressor on-off cycle based on these performance indicators. The total energy transferred from the air to the refrigerant in Joules was evaluated by taking the area under the curve for one compressor on-off cycle of the cooling plot described in Figure 5-5,

$$Q\ (kJ) = \int E(kW)\ dt \tag{17}$$

MATLAB command "trapz" was used to find the area under the cooling curve for the three control mechanisms. Similarly the total power consumed by the system was evaluated.

Table 5-1 Comparison of Performance Indicators for One Compressor On-Off Cycle for Each Actuator

	TEV	MS Controller	Cascaded Controller
Time On [s]	300	265	200
Time Off [s]	190	175	210
$\dot{Q}_{on}$ [kW]	5.21	7.30	7.56
$\dot{W}_{on}$ [kW]	2.26	2.27	2.27
$\dot{W}_{off}$ [kW]	0.46	0.46	0.46
Total Q_{on}[kJ]	12286	15985	14853
Total W_{on}[kJ]	6236.72	6106.44	4478.00
Total W_{off}[kJ]	852.16	714.32	1040.6
Duty Cycle [%]	61.22	60.22	48.78
COP_{on}	1.97	2.61	3.31
COP_{total}	1.73	2.34	2.69
COP Improvement compared to TEVs [%]	-	35.26 %	55.49%

The data points listed in the table above are for one-compressor on-off cycle. By analyzing this data, we find significant gain in the COP of the system with the use of the cascaded controller (+55.49 %) and the MS SHC (+35.26%) as compared to the TEVs. Also the duty cycle is least for the cascaded controller followed by the MS SHC and then the TEVs. It implies that if the unit runs for equal number of cycles in one day, we will observe that the compressor will remain shut off for more time period in case of the cascaded controller as compared to the MS SHC and the TEVs. This directly reflects substantial power savings for the designed cascaded superheat controller when the system runs for a longer time periods. Future work would include running the system for

longer time periods and at different operating conditions, day temperature, humidity level etc. and taking the average data values, which would allow us to accurately quantify the efficiency gains for the three actuating mechanisms.

The control architecture for the Microstaq SHC is unknown due to commercial confidentiality. The subsequent experiments on the MS SHC sometimes resulted in erratic fluctuations in the valve opening when the system is subjected to transient internal or external disturbances as shown in Figure 5-8.

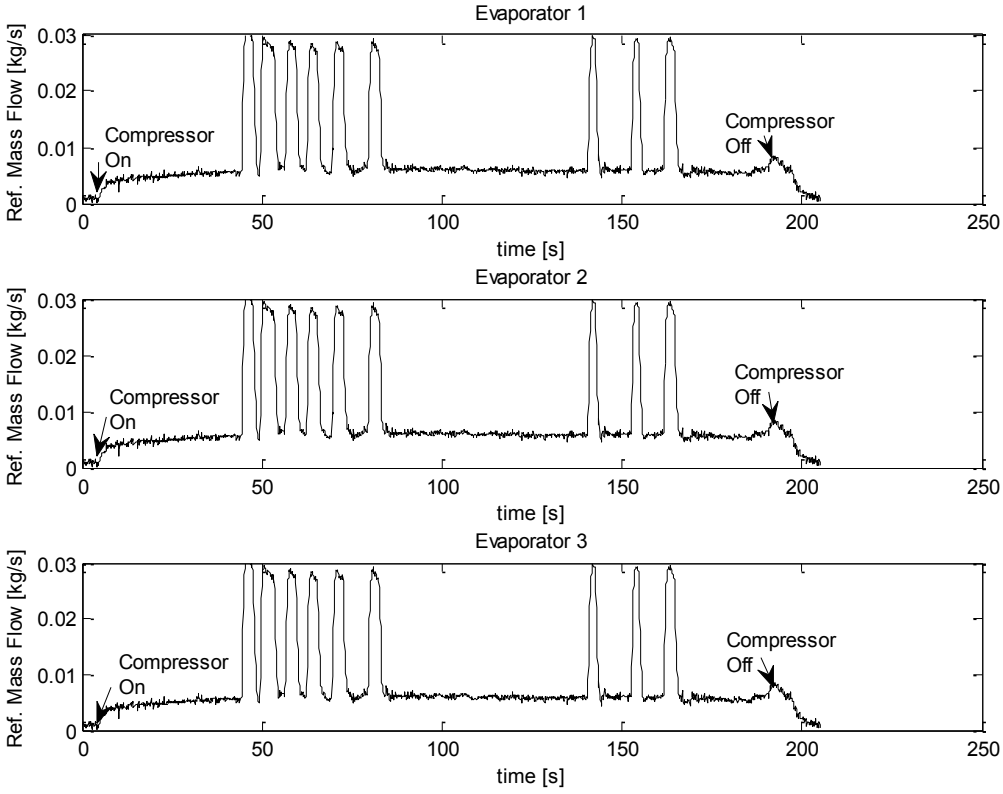

Figure 5-8 Instance of Random Fluctuation in Refrigerant Mass Flow Rate for MS Controller

As, shown above the refrigerant mass flow rate to the evaporators changed abruptly in the middle of the compressor run cycle, which corresponds to random

opening and closing of the valves. Hence the efficiency gains resulting from such behavior becomes difficult to quantify when a MS controller is used.

For the testing scenario discussed above, there are significant energy efficiency gains for the MS SHC and the cascaded controller over the mechanical TEVs. Between the MS SHC and the cascaded strategy, the performance of the cascaded controller is slightly better than the MS controller. But on few occasions, the MS SHC exhibited uncharacteristic behavior in cooling due to constant opening and closing of the valves as shown in Figure 5-9.

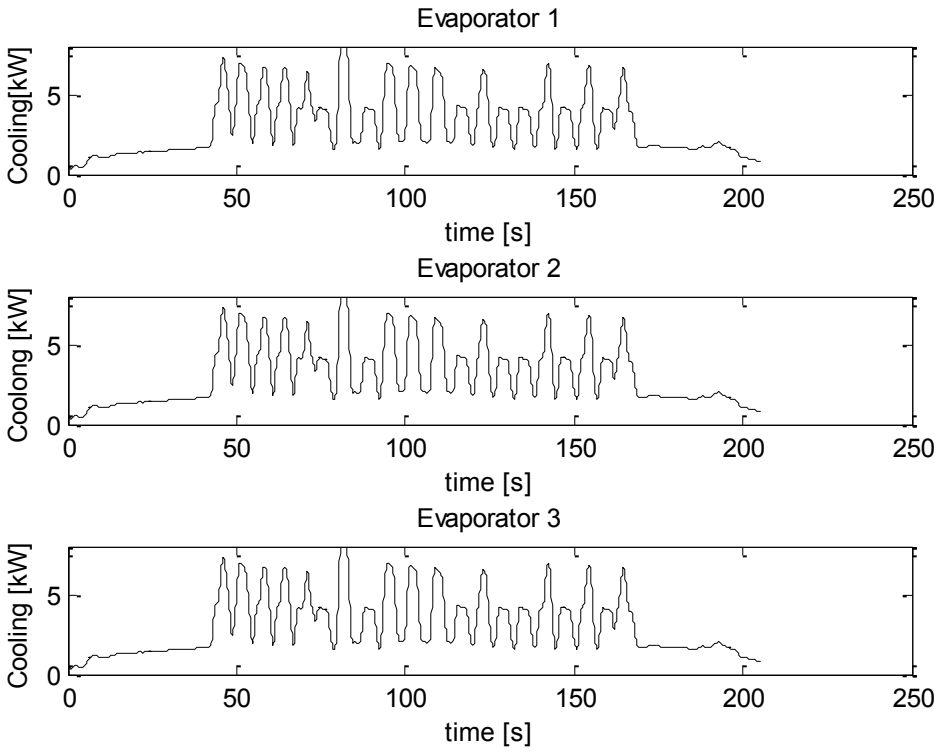

Figure 5-9 Instance of Random Fluctuations in Cooling for the MS Controller

These random fluctuations makes difficult to quantify average cooling and COP for the MS SHC. However, among all the three actuators the cascaded control architecture can be said to be the most effective one for the open display case in terms of regulating superheat at the set point, superior stable cooling and enhanced COP.

6. CONCLUSION AND FUTURE WORK

This thesis makes contribution towards modeling of the multi-evaporator systems based on the existing Moving Boundary Approach. The modeling methodology discussed for a three evaporator system is fairly simple and at the same time novel. This dynamic modeling technique can be generalized for any number of evaporators in an AC&R system. The models are validated by a commercial multi-evaporator supermarket open display case unit. Step tests are performed which indicate that models fairly capture the steady state and transient dynamics of the system.

This work also presents design of an effective cascaded controller on MEMS based Silicon Expansion Valves. The experiments conducted on the supermarket refrigeration system indicate energy gains when the commercial Microstaq Superheat and the cascaded controller are used over the standard Thermal Expansion Valves. The energy savings is attributed to the fact that the compressor run time is less for the Microstaq and the cascaded controller. The Microstaq SHC also showed oscillatory behavior at transient system startup with random opening and closing of the valves. The cascaded control architecture was better than the MS SHC in superheat reference point tracking and in some cases even superior cooling was observed.

Future research may continue on the multi-evaporator dynamic models including the modeling of the plate type condenser which was not done in this study. The models can be validated for step changes in the secondary fluid flow rate on the condenser side. More model validation can be done if a variable frequency drive compressor is used on

the system. The efficacy of the cascaded control can be observed if the three evaporators have different internal air temperatures and different evaporator fan speeds. This can be achieved by using a partition in the unit for the three evaporators and running each evaporator fan at different speed. The performance of the Microstaq SHC and cascaded controller can be further compared by precisely starting the system at similar ambient and operating condition. A meeting with the Microstaq personnel in context of rectifying the oscillatory behavior of their controller would also help in better analyzing the performance of the two controllers.

REFERENCES

[1] Center for Sustainable Systems, University of Michigan, Ann Arbor, MI, "Commercial buildings factsheet", *Publication No. CSS05-05*, 2011. [Online]. Available: http://css.snre.umich.edu/css_doc/CSS05-05.pdf

[2] Energy Star Building Manual, "Facility Type: Supermarkets and grocery stores", Chapter 11, January 2008. [Online]. Available: www.energystar.gov/ia/business/EPA_BUM_CH11_Supermarkets.pdf

[3] V. D. Baxter, "Advances in supermarket refrigeration systems", Oak Ridge National Laboratory, Oak Ridge, TN, March, 2011. [Online]. Available: http://www.arb.ca.gov/cc/commref/adv_supmkt_ref_syst.pdf

[4] J. Michaels and A. Swenson, "Commercial buildings energy consumption survey—Overview of commercial buildings characteristics", 2003. [Online]. Available: http://www.eia.gov/emeu/cbecs/cbecs2003/introduction.html

[5] Center for Compact and Efficient Fluid Power, University of Minnesota, Minneapolis, MN, "MEMS Proportional Pneumatic Valve", July, 2012. [Online]. Available: http://www.ccefp.org/research/thrust-2-compactness/project-2f

[6] Microstaq Inc., Austin , TX, "Silicon expansion valve v 2.1 datasheet", March 2011. [Online]. Available: http://www.microstaq.com/pub/docs/SEV_Datasheet_17_Mar_11.pdf

[7] M. Luckevich, "MEMS Microvalves: The new valve world", Microstaq Inc., May 2007. [Online]. Available: http://www.dunanmicrostaq.com/pub/docs/VW_MEMS_LR.pdf

[8] S. Bendapudi and J. E. Braun, "A review of literature on dynamic models of vapor compression equipment," *ASHRAE Report #4036-5*, May 2002.

[9] G. L Wedekind. and W. F. Stoecker, "Transient response of the mixture-vapor transition point in horizontal evaporating flow," *ASHRAE Transactions*, vol. 72, No.1, pp. 4.2.1-4.2.15, 1966.

[10] G.L. Wedekind, B.L. Bhatt and B.T. Beck, "A system mean void fraction model for predicting various transient phenomena associated with two-phase evaporating and condensing flows", *International Journal of Multiphase Flow*, vol. 4, Issue 1, pp. 97-114, March 1978.

[11] Eric W. Grald and J. Ward MacArthur, "A moving-boundary formulation for modeling time-dependent two phase flows", *International Journal of Heat and Fluid Flow*, vol. 13, Issue 3, pp. 266-272, September 1992.

[12] M.Dhar, "Transient analysis of refrigeration system", PhD Dissertation, Department of Mechanical Engineering, Purdue University, 1978.

[13] J.Chi and D.Didion, "A simulation model of the transient performance of heat pump", *International Journal of Refrigeration*, vol.5, pp. 176-184, 1982.

[14] W.D. Gruhle and R.Isermann, "Modeling and control of refrigerant evaporator", *Journal of Dynamic Systems, Measurement and Control*, vol. 107, pp. 235-240, 1985.

[15] M. Willatzen, N.B.O.L. Pettit and L. Ploug-Sørensen, "A general dynamic simulation model for evaporators and condensers in refrigeration. Part I: Moving-

boundary formulation of two-phase flows with heat exchanger", *International Journal of Refrigeration*, vol. 21, Issue 5, pp. 398-403, August 1998.

[16] B.P. Rasmussen, "Dynamic modeling and advanced control of air conditioning and refrigeration systems", PhD Dissertation, Deptartment of Mechanical Engineering, University of Illinois at Urbana Champaign, 2005.

[17] B.P Rasmussen, A.G. Alleyne and A. Musser, "Model driven system identification for transcritical vapor compression systems", *IEEE Transactions on Control Systems Technology*, vol.13, No. 3, pp. 444-451, May 2005.

[18] B.P. Rasmussen and A.Alleyne, "Control-oriented modeling of transcritical vapor compression systems", *ASME Journal of Dynamic Systems, Measurement and Control*, vol. 126, No.1, pp. 54-64, March, 2004.

[19] W. Zhang and C. Zhang, "A generalized moving-boundary model for transient simulation of dry-expansion evaporators under larger disturbances", *International Journal of Refrigeration*, vol. 29, pp. 1119-1127, 2006.

[20] A.Gupta, “Reduced order modeling of heat exchangers using high order finite control volume methods”, Master’s thesis, Department of Mechanical Engineering, Texas A&M University, 2007.

[21] B. Ayyagari, “Simulation and validation of vapor compressor system faults and start-up/shut-down transients”, Master’s thesis, Department of Mechanical Engineering, Texas A&M University, 2011.

[22] B.P. Rasmussen, “Review Article: Dynamic modeling of vapor compression systems – Part I: Literature Review”, *HVAC&R Research*, in review, 2010.

[23] B.P. Rasmussen and B. M. Shenoy, “Review Article: Dynamic modeling of vapor compression systems – Part II: Simulation Tutorial”, *HVAC&R Research*, in review, 2010.

[24] Chen Wu, Zhou Xingxi and Deng Shiming, "Development of control method and dynamic model for multi-evaporator air conditioners (MEAC*)", Energy Conversion and Management*, vol, 46, Issue 3, pp. 451-465, February 2005.

[25] Y.T. Ge and S.A. Tassour, "Mathematical modeling of supermarket refrigeration system for design, energy prediction and control", *Proceedings of Institution of Mechanical Engineers*, Part A 214, 2000.

[26] A.Thair and P.K. Bansal, "MPER versus EEPR valves in open supermarket refrigerated display cabinets", *Applied Thermal Engineering*, vol. 25, Issue 2-3, pp. 191-203, February, 2005.

[27] B.P. Rasmussen, B.Shenoy, E. Rodriguez, S. Liang, B. Ayyagari and N. Hariharan, “SBIR Report: Dynamic modeling library for vapor compression cycles”, *Report Unpublished*, Available at Thermo-Fluids Control Lab, Texas A&M University, 2011.

[28] J. P. Wattelet, "Heat transfer flow regimes of refrigerants in a horizontal - tube evaporator", *ACRC TR-55*,University of Illinois at Urbana-Champaign, 1994.

[29] V. Gnielinski, "New equation for heat and mass transfer in turbulent pipe and channel flow", *International Chemical Engineering,* vol. 16, pp. 359-368, 1976.

[30] M.S.Elliott, B.P.Rasmussen, Z. Bolding and B. Bolding, “Superheat control: A hybrid approach”, *HVAC&R Research*, vol. 15, no. 6, pp. 1021-1043, 2009.

[31] Jeff Uibel, “The miniaturization of flow control”, 9th International Symposium on Fluid Control, Measurement and Visualization (FLUCOME), Tallahassee, FL, 2007.

[32] M.S. Elliott and B. P.Rasmussen, “Evaporator superheat regulation via emulation of semi-active flow control”, *Proceedings of ASME Dynamic Systems and Control Conference*, Hollywood, CA, 2009.

[33] H. Rasmussen, T. Claus, L.F.S. Larsen, “Nonlinear superheat and temperature control of a refrigeration plant”, *IFAC ESC: Energy Savings Control in Plants and Buildings*, pp. 251-254, 2006.

[34] M.S. Elliott and B. P.Rasmussen, “On reducing evaporator superheat nonlinearity with control architecture”, *International Journal of Refrigeration*, vol. 33, Issue 3, pp. 607-614, May 2010.

[35] S.Skogestad and I.Postlethwaite, “*Multivariable Feedback control: Analysis and Design*”, 2nd edition, John Wiley & Sons Ltd., West Sussex, England, 2005, pp. 86-90.

[36] M.S. Elliott, C.Estrada and B.P. Rasmussen, “Cascaded superheat control with a multiple evaporator refrigeration system”, *Proceedings of American Control Conference,* San Francisco, CA, 2011.

APPENDIX A

A complete derivation of the mathematical equations for the evaporator modeling is given here. First of all, the parameters used in the derivation of the governing algebraic equations for the conservation of refrigeration mass, refrigeration energy and the wall energy are given in Table 1.

Table 1: Parameters Used in the Expansion of Conservation Equations

ρ	density of refrigerant (liquid phase and vapor phases denoted by ρ_f and ρ_g, respectively)
P	pressure of refrigerant
h	enthalpy of refrigerant (liquid phase and vapor phases denoted by h_f and h_g, respectively)
T_r	temperature of refrigerant
T_w	tube wall temperature
T_a	external air temperature
α_i	heat transfer coefficient between tube wall and internal fluid
α_o	heat transfer coefficient between tube wall and external fluid
A_{cs}	cross sectional area of the inside of the tube

A_i	internal surface area of the heat exchanger
A_o	external surface area of the heat exchanger
$\dot{m}$	mass flow rate of refrigerant flowing along the tube
$(C_p \rho V)_w$	thermal capacitance of the tube wall per unit length
$\bar{\gamma}$	mean void fraction
μ	weight factor for external air temperature

As discussed in Section 3, a moving boundary evaporator can be characterized by two control volumes, a two-phase liquid and a superheated state. For the external heat transfer, a weighted average of the air temperature across the evaporator is assumed as given in Equation 1. In the first region, the fluid properties are determined assuming a mean void fraction as shown in Equation 2 and 3 whereas in the second region average properties are assumed as shown in Equation 4.

$$T_a = T_{a,in}(\mu) + T_{a,out}(1-\mu) \tag{1}$$

$$\rho_1 = \rho_f(1-\bar{\gamma}) + \rho_g(\bar{\gamma}) \tag{2}$$

$$\rho h = \rho_f h_f(1-\bar{\gamma}) + \rho_g h_g \bar{\gamma} \tag{3}$$

$$h_2 = \frac{h_g + h_{out}}{2}, \quad T_{r2} = T(P_e, h_2), \quad \rho_2 = \rho(P_e, h_2) \tag{4}$$

Again as discussed in Section 3 of this thesis, the equations are derived from the expression for conservation of refrigerant mass (Equations 5 - 7), refrigerant energy (Equations 8 - 10) and the wall energy (Equations 11 - 13) for each of the control volume of the moving boundary evaporator. The wall temperature at the interface is calculated as a weighted mean of the wall temperatures in the two phase and the superheated regions, i.e. $T_{w,int} = \frac{L_2}{L} T_{w,1} + \frac{L_1}{L} T_{w,2}$ [16].

Conservation of refrigerant mass for two phase and superheated region

$$\frac{\partial(\rho A_{cs})}{\partial t} + \frac{\partial \dot{m}}{\partial z} = 0 \tag{5}$$

Integrated form:

$$A_{cs}L_1\left[\frac{d\rho_f}{dP_e}(1-\bar{\gamma}) + \frac{d\rho_g}{dP_e}\bar{\gamma} + (\rho_g - \rho_f)\frac{\partial \bar{\gamma}}{\partial P_e}\right]\dot{P}_e + A_{cs}(\rho_f - \rho_g)(1-\bar{\gamma})\dot{L}_1 = \dot{m}_{r,i} - \dot{m}_{r,int} \tag{6}$$

$$A_{cs}L_2\left[\frac{\partial \rho_{r,2}}{\partial P_e} + \frac{1}{2}\frac{\partial \rho_{r,2}}{\partial h_{r,2}}\frac{dh_g}{dP_e}\right]\dot{P}_e + A_{cs}(\rho_g - \rho_{r,2})\,\dot{L}_1 + A_{cs}L_2\frac{1}{2}\frac{\partial \rho_{r,2}}{\partial h_{r,2}}\dot{h}_{out} = \dot{m}_{r,int} - \dot{m}_{r,o} \tag{7}$$

Conservation of refrigerant energy for two phase and superheated region

$$\frac{\partial(\rho A_{cs} h - A_{cs} P)}{\partial t} + \frac{\partial(\dot{m} h)}{\partial z} = p_i \alpha_i (T_w - T_r) \tag{8}$$

Integrated form:

$$\begin{aligned} A_{cs} L_1 \left[\frac{d(\rho_f h_f)}{dP_e}(1-\bar{\gamma}) + \frac{d(\rho_g h_g)}{dP_e}\bar{\gamma} + (\rho_g h_g - \rho_f h_f)\frac{\partial \bar{\gamma}}{\partial P_e} - 1 \right] \dot{P}_e \\ + A_{cs}(\rho_f h_f - \rho_g h_g)(1-\bar{\gamma})\dot{L}_1 \\ = \dot{m}_{r,i} h_{r,i} - \dot{m}_{r,int} h_{r,int} + \alpha_{i1} A_i \left(\frac{L_1}{L_{total}}\right)(T_{w1} - T_{r1}) \end{aligned} \tag{9}$$

$$\begin{aligned} A_{cs} L_2 \left[\left(\frac{\partial \rho_{r,2}}{\partial P_e} + \frac{1}{2}\frac{\partial \rho_{r,2}}{\partial h_{r,2}}\frac{dh_g}{dP_e} \right) h_{r,2} + \frac{1}{2}\frac{dh_g}{dP_e}\rho_{r,2} - 1 \right] \dot{P}_e \\ + A_{cs}(\rho_g h_g - \rho_{r,2} h_{r,2})\dot{L}_1 \\ + A_{cs} L_2 \left(\frac{1}{2}\right)\left[\frac{\partial \rho_{r,2}}{\partial h_{r,2}} h_{r,2} + \rho_{r,2} \right] \dot{h}_{out} \\ = \dot{m}_{r,int} h_{r,int} - \dot{m}_{r,o} h_{r,o} + \alpha_{i2} A_i \left(\frac{L_2}{L_{total}}\right)(T_{w2} - T_{r2}) \end{aligned} \tag{10}$$

Conservation of wall energy two phase and superheated region

$$\left(C_p \rho A\right)_w \frac{\partial (T_w)}{\partial t} = p_i \alpha_i (T_r - T_w) + p_o \alpha_o (T_a - T_w) \tag{11}$$

Integrated form:

$$\left(C_p \rho V\right)_w \left[\dot{T}_{w,1} + \frac{T_{w,1} - T_{w,int}}{L_1} \dot{L}_1\right] = \alpha_{i1} A_i \left(T_{r,1} - T_{w,1}\right) + \alpha_o A_o \left(T_a - T_{w,1}\right) \tag{12}$$

$$\left(C_p \rho V\right)_w \left[\dot{T}_{w,1} + \frac{T_{w,1} - T_{w,int}}{L_1} \dot{L}_1\right] = \alpha_{i1} A_i \left(T_{r,1} - T_{w,1}\right) + \alpha_o A_o \left(T_a - T_{w,1}\right) \tag{13}$$

The conservation of mass equations (6-7) for the single evaporator can be combined to eliminate the interface mass flow rate and get a single equation. This gives us five key equations for a single evaporator (one equation for the conservation of mass, two integrated form equations for the conservation of refrigerant energy in the superheat and the two-phase regions and the last two equations for the conservation of wall energy in the superheated and the two phase region).

Now the same sets of equations were written again for 3 different evaporators which are connected in parallel with the superscripts 1, 2 and 3. The superscripts represent evaporators 1, 2 and 3 respectively. This representation is used throughout this Appendix. Again, the two assumptions as described in Section 3 can be re-written in the form of equations 14, 15 and 16.

$$\dot{P}_e^{\,1} - \dot{P}_e^{\,2} = 0 \tag{14}$$

$$\dot{P_e}^2 - \dot{P_e}^3 = 0 \tag{15}$$

$$\dot{m}_{out}{}^1 + \dot{m}_{out}{}^2 + \dot{m}_{out}{}^3 = \dot{m}_{comp.} \tag{16}$$

Finally we get 18 equations, five governing equations for the individual evaporators and three equations (14-16) for combining the three evaporators. All the equations for the three evaporators can be combined to express it in the form $Z(x,u)\dot{x} = f(x,u)$. The state vector x now consists of 18 elements as expressed below,

$$x = [L_1{}^1 \quad P_e{}^1 \quad h_{out}{}^1 \quad T_{wall,1}{}^1 \quad T_{wall,2}{}^1 \; m_{out}{}^1 \; L_1{}^2 \quad P_e{}^2 \quad h_{out}{}^2 \quad T_{wall,1}{}^2 \quad T_{wall,2}{}^2$$

$$m_{out}{}^2 \; L_1{}^3 \quad P_e{}^3 \quad h_{out}{}^3 \quad T_{wall,1}{}^3 \quad T_{wall,2}{}^3 \; m_{out}{}^3 \;] .$$

Equation 17 shows the state space representation of the evaporator model and Table 2 gives the elements of the Z matrix,

$$
\begin{bmatrix}
z_{11} & z_{12} & z_{13} & 0 & 0 & z_{16} & 0 & 0 & 0 & 0 & 0 & 0 & 0 & 0 & 0 & 0 & 0 & 0 \\
z_{21} & z_{21} & z_{23} & 0 & 0 & z_{26} & 0 & 0 & 0 & 0 & 0 & 0 & 0 & 0 & 0 & 0 & 0 & 0 \\
z_{31} & z_{32} & z_{33} & 0 & 0 & z_{36} & 0 & 0 & 0 & 0 & 0 & 0 & 0 & 0 & 0 & 0 & 0 & 0 \\
z_{41} & 0 & 0 & z_{44} & 0 & 0 & 0 & 0 & 0 & 0 & 0 & 0 & 0 & 0 & 0 & 0 & 0 & 0 \\
z_{51} & 0 & 0 & 0 & z_{55} & 0 & 0 & 0 & 0 & 0 & 0 & 0 & 0 & 0 & 0 & 0 & 0 & 0 \\
0 & z_{62} & 0 & 0 & 0 & 0 & 0 & z_{68} & 0 & 0 & 0 & 0 & 0 & 0 & 0 & 0 & 0 & 0 \\
0 & 0 & 0 & 0 & 0 & 0 & z_{77} & z_{78} & z_{79} & 0 & 0 & z_{7\,12} & 0 & 0 & 0 & 0 & 0 & 0 \\
0 & 0 & 0 & 0 & 0 & 0 & z_{87} & z_{88} & z_{89} & 0 & 0 & z_{8\,12} & 0 & 0 & 0 & 0 & 0 & 0 \\
0 & 0 & 0 & 0 & 0 & 0 & z_{97} & z_{98} & z_{99} & 0 & 0 & z_{9\,12} & 0 & 0 & 0 & 0 & 0 & 0 \\
0 & 0 & 0 & 0 & 0 & 0 & z_{10\,7} & 0 & 0 & z_{10\,10} & 0 & 0 & 0 & 0 & 0 & 0 & 0 & 0 \\
0 & 0 & 0 & 0 & 0 & 0 & z_{11\,7} & 0 & 0 & 0 & z_{11\,11} & 0 & 0 & 0 & 0 & 0 & 0 & 0 \\
0 & 0 & 0 & 0 & 0 & 0 & 0 & 0 & 0 & 0 & 0 & 0 & z_{12\,13} & z_{12\,14} & z_{12\,15} & 0 & 0 & z_{12\,18} \\
0 & 0 & 0 & 0 & 0 & 0 & 0 & 0 & 0 & 0 & 0 & 0 & z_{13\,13} & z_{13\,14} & z_{13\,15} & 0 & 0 & z_{13\,18} \\
0 & 0 & 0 & 0 & 0 & 0 & 0 & 0 & 0 & 0 & 0 & 0 & z_{14\,13} & z_{14\,14} & z_{14\,15} & 0 & 0 & z_{14\,18} \\
0 & 0 & 0 & 0 & 0 & 0 & 0 & 0 & 0 & 0 & 0 & 0 & z_{15\,13} & 0 & 0 & z_{15\,16} & 0 & 0 \\
0 & 0 & 0 & 0 & 0 & 0 & 0 & 0 & 0 & 0 & 0 & 0 & z_{16\,13} & 0 & 0 & 0 & z_{16\,17} & 0 \\
0 & 0 & 0 & 0 & 0 & 0 & 0 & z_{17\,8} & 0 & 0 & 0 & 0 & 0 & z_{17\,14} & 0 & 0 & 0 & 0 \\
0 & 0 & 0 & 0 & 0 & z_{18\,6} & 0 & 0 & 0 & 0 & 0 & z_{18\,12} & 0 & 0 & 0 & 0 & 0 & z_{18\,18}
\end{bmatrix}
\begin{bmatrix}
\dot{L_1}^1 \\ \dot{P_e}^1 \\ \dot{h_{out}}^1 \\ \dot{T}_{wall,1}{}^1 \\ \dot{T}_{wall,2}{}^1 \\ \dot{m}_{out}{}^1 \\ \dot{L_1}^2 \\ \dot{P_e}^2 \\ \dot{h_{out}}^2 \\ \dot{T}_{wall,1}{}^2 \\ \dot{T}_{wall,2}{}^2 \\ \dot{m}_{out}{}^2 \\ \dot{L_1}^3 \\ \dot{P_e}^3 \\ \dot{h_{out}}^3 \\ \dot{T}_{wall,1}{}^3 \\ \dot{T}_{wall,2}{}^3 \\ \dot{m}_{out}{}^3
\end{bmatrix}
$$

$$
= \begin{bmatrix}
\dot{m}_{r,i}{}^1 h_{r,i}{}^1 + \alpha_{i1}{}^1 A_i{}^1 \left(\frac{L_1{}^1}{L_{total}{}^1}\right)\left(T_{w1}{}^1 - T_{r1}{}^1\right) \\
\alpha_{i2}{}^1 A_i{}^1 \left(\frac{L_2{}^1}{L_{total}{}^1}\right)\left(T_{w2}{}^1 - T_{r2}{}^1\right) \\
\dot{m}_{r,i}{}^1 \\
\alpha_{i1}{}^1 A_i{}^1 \left(T_{r,1}{}^1 - T_{w,1}{}^1\right) + \alpha_o{}^1 A_o{}^1 \left(T_a{}^1 - T_{w,1}{}^1\right) \\
\alpha_{i2}{}^1 A_i{}^1 \left(T_{r,2}{}^1 - T_{w,2}{}^1\right) + \alpha_o{}^1 A_o{}^1 \left(T_a{}^1 - T_{w,2}{}^1\right) \\
0 \\
\dot{m}_{r,i}{}^2 h_{r,i}{}^2 + \alpha_{i1}{}^2 A_i{}^2 \left(\frac{L_1{}^2}{L_{total}{}^2}\right)\left(T_{w1}{}^2 - T_{r1}{}^2\right) \\
\alpha_{i2}{}^2 A_i{}^2 \left(\frac{L_2{}^2}{L_{total}{}^2}\right)\left(T_{w2}{}^2 - T_{r2}{}^2\right) \\
\dot{m}_{r,i}{}^2 \\
\alpha_{i1}{}^2 A_i{}^2 \left(T_{r,1}{}^2 - T_{w,1}{}^2\right) + \alpha_o{}^2 A_o{}^2 \left(T_a{}^2 - T_{w,1}{}^2\right) \\
\alpha_{i2}{}^2 A_i{}^2 \left(T_{r,2}{}^2 - T_{w,2}{}^2\right) + \alpha_o{}^2 A_o{}^2 \left(T_a{}^2 - T_{w,2}{}^2\right) \\
\dot{m}_{r,i}{}^3 h_{r,i}{}^3 + \alpha_{i1}{}^3 A_i{}^3 \left(\frac{L_1{}^3}{L_{total}{}^3}\right)\left(T_{w1}{}^3 - T_{r1}{}^3\right) \\
\alpha_{i2}{}^3 A_i{}^3 \left(\frac{L_2{}^3}{L_{total}{}^3}\right)\left(T_{w2}{}^3 - T_{r2}{}^3\right) \\
\dot{m}_{r,i}{}^3 \\
\alpha_{i1}{}^3 A_i{}^3 \left(T_{r,1}{}^3 - T_{w,1}{}^3\right) + \alpha_o{}^3 A_o{}^3 \left(T_a{}^3 - T_{w,1}{}^3\right) \\
\alpha_{i2}{}^3 A_i{}^3 \left(T_{r,2}{}^3 - T_{w,2}{}^3\right) + \alpha_o{}^3 A_o{}^3 \left(T_a{}^3 - T_{w,2}{}^3\right) \\
0 \\
\dot{m}_{comp.}
\end{bmatrix} \tag{17}
$$

Table 2 Matrix Elements of $\boldsymbol{Z(x,u)}$.

z_{11}	$A_{cs}{}^{1}\left[\left(\rho_f{}^{1}h_f{}^{1}-\rho_g{}^{1}h_g{}^{1}\right)\left(1-\bar{\gamma}^{1}\right)+h_g{}^{1}\left(\rho_g{}^{1}-\rho_{r,2}{}^{1}\right)\right]$
z_{12}	$A_{cs}{}^{1}L_1{}^{1}\left[\frac{d\left(\rho_f h_f\right)^{1}}{dP_e}\left(1-\bar{\gamma}^{1}\right)+\frac{d\left(\rho_g h_g\right)^{1}}{dP_e}\bar{\gamma}^{1}+\left(\rho_g{}^{1}h_g{}^{1}-\rho_f{}^{1}h_f{}^{1}\right)\frac{\partial\bar{\gamma}^{1}}{\partial P_e}-1\right]+A_{cs}{}^{1}L_2{}^{1}h_g{}^{1}\left(\frac{\partial\rho_{r,2}{}^{1}}{\partial P_e}+\frac{1}{2}\frac{\partial\rho_{r,2}{}^{1}}{\partial h_{r,2}}\frac{dh_g{}^{1}}{dP_e}\right)$
z_{13}	$A_{cs}{}^{1}L_2{}^{1}h_g{}^{1}\left(\frac{1}{2}\frac{\partial\rho_{r,2}}{\partial h_{r,2}}\right)^{1}$
z_{16}	$h_g{}^{1}$
z_{21}	$A_{cs}{}^{1}\rho_{r,2}{}^{1}\left(h_g{}^{1}-h_{r,2}{}^{1}\right)$
z_{22}	$A_{cs}{}^{1}L_2{}^{1}\left[\left(\frac{\partial\rho_{r,2}{}^{1}}{\partial P_e}+\frac{1}{2}\frac{\partial\rho_{r,2}{}^{1}}{\partial h_{r,2}}\frac{dh_g{}^{1}}{dP_e}\right)\left(h_{r,2}{}^{1}-h_g{}^{1}\right)+\frac{1}{2}\frac{dh_g{}^{1}}{dP_e}\rho_{r,2}{}^{1}-1\right]$
z_{23}	$A_{cs}{}^{1}L_2{}^{1}\frac{1}{2}\left[\frac{\partial\rho_{r,2}{}^{1}}{\partial h_{r,2}}\left(h_{r,2}{}^{1}-h_g{}^{1}\right)+\rho_{r,2}{}^{1}\right]$
z_{26}	$h_{ro}{}^{1}-h_g{}^{1}$
z_{31}	$A_{cs}{}^{1}\left[\left(\rho_f{}^{1}-\rho_g{}^{1}\right)\left(1-\bar{\gamma}^{1}\right)+\left(\rho_g{}^{1}-\rho_{r,2}{}^{1}\right)\right]$
z_{32}	$A_{cs}{}^{1}L_1{}^{1}\left[\frac{\partial\rho_f{}^{1}}{\partial P_e}\left(1-\bar{\gamma}^{1}\right)+\frac{\partial\rho_g{}^{1}}{\partial P_e}\bar{\gamma}^{1}+\left(\rho_g{}^{1}-\rho_f{}^{1}\right)\frac{\partial\bar{\gamma}^{1}}{\partial P_e}\right]+A_{cs}{}^{1}L_2{}^{1}\left(\frac{\partial\rho_{r,2}{}^{1}}{\partial P_e}+\frac{1}{2}\frac{\partial\rho_{r,2}{}^{1}}{\partial h_{r,2}}\frac{dh_g{}^{1}}{dP_e}\right)$
z_{33}	$A_{cs}{}^{1}L_2{}^{1}\left(\frac{1}{2}\frac{\partial\rho_{r,2}{}^{1}}{\partial h_{r,2}}\right)$
z_{36}	1

z_{41}	$\left(C_p\rho V\right)^1{}_w \dfrac{{T_{w,1}}^1 - {T_{w,int}}^1}{{L_1}^1}$
z_{44}	$\left(C_p\rho V\right)^1{}_w$
z_{51}	$\left(C_p\rho V\right)^1{}_w \dfrac{{T_{w,int}}^1 - {T_{w,2}}^1}{{L_2}^1}$
z_{55}	$\left(C_p\rho V\right)^1{}_w$
z_{62}	1
z_{68}	-1
z_{77}	${A_{cs}}^2\left[\left({\rho_f}^2{h_f}^2 - {\rho_g}^2{h_g}^2\right)\left(1-\bar{\gamma}^2\right) + {h_g}^2\left({\rho_g}^2 - {\rho_{r,2}}^2\right)\right]$
z_{78}	${A_{cs}}^2{L_1}^2\left[\dfrac{d\left(\rho_f h_f\right)^2}{dP_e}\left(1-\bar{\gamma}^2\right) + \dfrac{d\left(\rho_g h_g\right)^2}{dP_e}\bar{\gamma}^2 + \left({\rho_g}^2{h_g}^2 - {\rho_f}^2{h_f}^2\right)\dfrac{\partial\bar{\gamma}^2}{\partial P_e} - 1\right] + {A_{cs}}^2{L_2}^2{h_g}^2\left(\dfrac{\partial{\rho_{r,2}}^2}{\partial P_e} + \dfrac{1}{2}\dfrac{\partial{\rho_{r,2}}^2}{\partial h_{r,2}}\dfrac{d{h_g}^2}{dP_e}\right)$
z_{79}	${A_{cs}}^2{L_2}^2{h_g}^2\left(\dfrac{1}{2}\dfrac{\partial\rho_{r,2}}{\partial h_{r,2}}\right)^2$
$z_{7\,12}$	${h_g}^2$
z_{87}	${A_{cs}}^2{\rho_{r,2}}^2\left({h_g}^2 - {h_{r,2}}^2\right)$
z_{88}	${A_{cs}}^2{L_2}^2\left[\left(\dfrac{\partial{\rho_{r,2}}^2}{\partial P_e} + \dfrac{1}{2}\dfrac{\partial{\rho_{r,2}}^2}{\partial h_{r,2}}\dfrac{d{h_g}^2}{dP_e}\right)\left({h_{r,2}}^2 - {h_g}^2\right) + \dfrac{1}{2}\dfrac{d{h_g}^2}{dP_e}{\rho_{r,2}}^2 - 1\right]$
z_{89}	${A_{cs}}^2{L_2}^2\dfrac{1}{2}\left[\dfrac{\partial{\rho_{r,2}}^2}{\partial h_{r,2}}\left({h_{r,2}}^2 - {h_g}^2\right) + {\rho_{r,2}}^2\right]$
$z_{8\,12}$	${h_{ro}}^2 - {h_g}^2$

z_{97}	$A_{cs}{}^2\left[\left(\rho_f{}^2-\rho_g{}^2\right)\left(1-\bar{\gamma}^2\right)+\left(\rho_g{}^2-\rho_{r,2}{}^2\right)\right]$
z_{98}	$A_{cs}{}^2 L_1{}^2\left[\frac{\partial\rho_f{}^2}{\partial P_e}\left(1-\bar{\gamma}^2\right)+\frac{\partial\rho_g{}^2}{\partial P_e}\bar{\gamma}^2+\left(\rho_g{}^2-\rho_f{}^2\right)\frac{\partial\bar{\gamma}^2}{\partial P_e}\right]$ $+A_{cs}{}^2 L_2{}^2\left(\frac{\partial\rho_{r,2}{}^2}{\partial P_e}+\frac{1}{2}\frac{\partial\rho_{r,2}{}^2}{\partial h_{r,2}}\frac{dh_g{}^2}{dP_e}\right)$
z_{99}	$A_{cs}{}^2 L_2{}^2\left(\frac{1}{2}\frac{\partial\rho_{r,2}{}^2}{\partial h_{r,2}}\right)$
$z_{9\,12}$	1
$z_{10\,7}$	$\left(C_p\rho V\right)_w^2\frac{T_{w,1}{}^2-T_{w,int}{}^2}{L_1{}^2}$
$z_{10\,10}$	$\left(C_p\rho V\right)_w^2$
$z_{11\,7}$	$\left(C_p\rho V\right)_w^2\frac{T_{w,int}{}^2-T_{w,2}{}^2}{L_2{}^1}$
$z_{11\,11}$	$\left(C_p\rho V\right)_w^2$
$z_{12\,13}$	$A_{cs}{}^3\left[\left(\rho_f{}^3 h_f{}^3-\rho_g{}^3 h_g{}^3\right)\left(1-\bar{\gamma}^3\right)+h_g{}^3\left(\rho_g{}^3-\rho_{r,2}{}^3\right)\right]$
$z_{12\,14}$	$A_{cs}{}^3 L_1{}^3\left[\frac{d\left(\rho_f h_f\right)^3}{dP_e}\left(1-\bar{\gamma}^3\right)+\frac{d\left(\rho_g h_g\right)^3}{dP_e}\bar{\gamma}^3+\left(\rho_g{}^3 h_g{}^3-\rho_f{}^3 h_f{}^3\right)\frac{\partial\bar{\gamma}^3}{\partial P_e}\right.$ $\left.-1\right]+A_{cs}{}^3 L_2{}^3 h_g{}^3\left(\frac{\partial\rho_{r,2}{}^3}{\partial P_e}+\frac{1}{2}\frac{\partial\rho_{r,2}{}^3}{\partial h_{r,2}}\frac{dh_g{}^3}{dP_e}\right)$
$z_{12\,15}$	$A_{cs}{}^3 L_2{}^3 h_g{}^3\left(\frac{1}{2}\frac{\partial\rho_{r,2}}{\partial h_{r,2}}\right)^3$
$z_{12\,18}$	$h_g{}^3$

$z_{13\,13}$	$A_{cs}{}^{3}\rho_{r,2}{}^{3}\left(h_g{}^{3}-h_{r,2}{}^{3}\right)$
$z_{13\,14}$	$A_{cs}{}^{3}L_2{}^{3}\left[\left(\frac{\partial\rho_{r,2}}{\partial P_e}^{3}+\frac{1}{2}\frac{\partial\rho_{r,2}}{\partial h_{r,2}}^{3}\frac{dh_g}{dP_e}^{3}\right)\left(h_{r,2}{}^{3}-h_g{}^{3}\right)+\frac{1}{2}\frac{dh_g}{dP_e}^{3}\rho_{r,2}{}^{3}-1\right]$
$z_{13\,15}$	$A_{cs}{}^{3}L_2{}^{3}\frac{1}{2}\left[\frac{\partial\rho_{r,2}}{\partial h_{r,2}}^{3}\left(h_{r,2}{}^{3}-h_g{}^{3}\right)+\rho_{r,2}{}^{3}\right]$
$z_{13\,18}$	$h_{ro}{}^{3}-h_g{}^{3}$
$z_{14\,13}$	$A_{cs}{}^{3}\left[\left(\rho_f{}^{3}-\rho_g{}^{3}\right)\left(1-\bar{\gamma}^3\right)+\left(\rho_g{}^{3}-\rho_{r,2}{}^{3}\right)\right]$
$z_{14\,14}$	$A_{cs}{}^{3}L_1{}^{3}\left[\frac{\partial\rho_f}{\partial P_e}^{3}\left(1-\bar{\gamma}^3\right)+\frac{\partial\rho_g}{\partial P_e}^{3}\bar{\gamma}^3+\left(\rho_g{}^{3}-\rho_f{}^{3}\right)\frac{\partial\bar{\gamma}}{\partial P_e}^{3}\right]$ $+A_{cs}{}^{3}L_2{}^{3}\left(\frac{\partial\rho_{r,2}}{\partial P_e}^{3}+\frac{1}{2}\frac{\partial\rho_{r,2}}{\partial h_{r,2}}^{3}\frac{dh_g}{dP_e}^{3}\right)$
$z_{14\,15}$	$A_{cs}{}^{3}L_2{}^{3}\left(\frac{1}{2}\frac{\partial\rho_{r,2}}{\partial h_{r,2}}^{3}\right)$
$z_{14\,18}$	1
$z_{15\,13}$	$\left(C_p\rho V\right)_w^3\frac{T_{w,1}{}^{3}-T_{w,int}{}^{3}}{L_1{}^{3}}$
$z_{15\,16}$	$\left(C_p\rho V\right)_w^3$
$z_{16\,13}$	$\left(C_p\rho V\right)_w^3\frac{T_{w,int}{}^{3}-T_{w,2}{}^{3}}{L_2{}^{3}}$
$z_{16\,17}$	$\left(C_p\rho V\right)_w^3$
$z_{17\,8}$	1
$z_{17\,14}$	-1

$z_{18\ 6}$	1
$z_{18\ 12}$	1
$z_{18\ 18}$	1